

Bulletin of the Iranian Mathematical Society
Assessing the impact of optimal control measures of COVID-19 and malaria co-morbidity: A dynamics modeling approach
--Manuscript Draft--

Manuscript Number:	BIMS-D-24-01000
Full Title:	Assessing the impact of optimal control measures of COVID-19 and malaria co-morbidity: A dynamics modeling approach
Article Type:	Original Article
Section/Category:	Dynamical System, Differential Equations and Control
Funding Information:	
Abstract:	<p>A mathematical model was developed in this study to examine the health impact of the mixed infection of malaria and COVID-19. Our aim is to understand the burden of disease for people who are co-infected with both COVID-19 and malaria, compared to those who are infected with either COVID-19 or malaria alone. Furthermore, we examined the synergistic connection between these two infections in the presence of various control measures. Initially, we analyze the states of mono-infection, calculate the baseline reproduction numbers, and study the local and global stability of disease-free equilibria. We also explore the influence of COVID-19 treatment and prevention measures, such as vaccination, on the dynamics of malaria. Thereafter, time dependent controls was introduced into the model by applying Maximum Principle developed by Pontryagin. This allows us to determine the conditions required for optimal disease control. Through our analysis, we discover that individuals infected with COVID-19 are at an elevated risk of contracting malaria, and vice versa. Moreover, those who are co-infected experience a rapid progression of both COVID-19 and malaria, bearing a heavier burden compared to individuals with single infections. To effectively manage the spread of COVID-19, malaria, and their co-infection, it is crucial for policymakers to promote the implementation of multiple intervention strategies. These strategies should address the control and prevention of both diseases simultaneously.</p>
Corresponding Author:	Akindele Onifade Mountain Top University NIGERIA
Corresponding Author Secondary Information:	
Corresponding Author's Institution:	Mountain Top University
Corresponding Author's Secondary Institution:	
First Author:	Akindele Onifade
First Author Secondary Information:	
Order of Authors:	Akindele Onifade Paul Odeniran, PhD Olatunde Ibrahim, PhD Isaiah Ademola, PhD
Order of Authors Secondary Information:	
Author Comments:	no comment
Suggested Reviewers:	Salihu Onifade, PhD Senior Researcher, University of Massachusetts Medical School Salihu.Musa@umassmed.edu He is an expert in mathematical biology Abdulaziz, Mukhtar, PhD

Lecturer, University of the Western Cape amukhtar@uwc.ac.za He is an expert in Mathematical biology
Winston Garira, PhD Full Professor, Sol Plaatje University winston.garira@spu.ac.za Sol Plaatje University, Private
Obiora Collins, PhD Senior Researcher, Durban University of Technology obiora.c.collins@gmail.com He is an expert in Mathematical Epidemiology
Mayowa Ojo, PhD Lecturer, Kansas State University mmojomth@gmail.com He is an expert in Mathematical Biology

[Click here to view linked References](#)

1

Assessing the impact of optimal control measures of COVID-19 and malaria co-morbidity: A dynamics modeling approach

Akindele Akano Onifade^{a,*}, Paul Olalekan Odeniran^b, Olatunde Emmanuel Ibrahim^c,
Isaiah Oluwafemi Ademola^b

^a*Department of Computer Science and Mathematics, Mountain Top University, Nigeria*

^b*Department of Veterinary Parasitology and Entomology, Faculty of Veterinary Medicine, University of Ibadan, Nigeria*

^c*Department of Infectious Disease Epidemiology, Imperial College London, United Kingdom*

15

16

17

18

19

20

21

22

23

24

25

26

27

28

29

30

31

32

33

34

35

36

37

38

39

40

41

42

43

44

45

46

47

48

49

50

51

52

53

54

55

56

57

58

59

60

61

62

63

64

65

Abstract

A mathematical model was developed in this study to examine the health impact of the mixed infection of malaria and COVID-19. Our aim is to understand the burden of disease for people who are co-infected with both COVID-19 and malaria, compared to those who are infected with either COVID-19 or malaria alone. Furthermore, we examined the synergistic connection between these two infections in the presence of various control measures. Initially, we analyze the states of mono-infection, calculate the baseline reproduction numbers, and study the local and global stability of disease-free equilibria. We also explore the influence of COVID-19 treatment and prevention measures, such as vaccination, on the dynamics of malaria. Thereafter, time dependent controls was introduced into the model by applying Maximum Principle developed by Pontryagin. This allows us to determine the conditions required for optimal disease control. Through our analysis, we discover that individuals infected with COVID-19 are at an elevated risk of contracting malaria, and vice versa. Moreover, those who are co-infected experience a rapid progression of both COVID-19 and malaria, bearing a heavier burden compared to individuals with single infections. To effectively manage the spread of COVID-19, malaria, and their co-infection, it is crucial for policymakers to promote the implementation of multiple intervention strategies. These strategies should address the control and prevention of both diseases simultaneously.

Keywords: Co-infection; COVID-19; Malaria; Optimal control; Reproduction number; Optimal control; Stability

2000 MSC: 37N25, 34C23, 49J15, 92D30

1. Introduction

The emergence of the coronavirus (SARS-CoV-2), leading to the COVID-19 pandemic, has generated an unprecedented public health crisis on a global scale.[1]. In January 2020, the World Health Organization (WHO) declared it a public health emergency of international concern, later upgrading it to a pandemic in March 2020. The severity of the outbreak was attributed to the significantly high basic reproduction number of the novel coronavirus, ranging from 2.24 to 3.58 [2]. It is worth noting that the symptoms of malaria and COVID-19

*Corresponding author

Email address: aaronifade@mtu.edu.ng (Akindele Akano Onifade)

can overlap, making it challenging to differentiate between the two. Common symptoms shared by these diseases include pyrexia, dyspnoea, lethargy and head aches. This similarity can lead to misdiagnosis of malaria as COVID-19, and vice versa, especially when clinicians heavily rely on symptoms alone. Additionally, the effectiveness of several older antimalarial drugs, both for treatment and prevention, is declining due to drug-resistant parasites. Consequently, the primary method of preventing malaria remains the use of bed nets to protect individuals at risk.

In the face of these challenges, policymakers are confronted with difficult decisions to effectively address urgent and ongoing public health issues, such as COVID-19 and endemic malaria, while minimizing the risks of infection. The current data showed a lower incidence of SARS-CoV-2 in developing countries, although the number of positive cases kept increasing on a daily basis in these areas. Incidentally, malaria disease is quite endemic in most of these developing countries especially Africa, of which the overburdened health systems aimed at curbing the SARS-CoV-2 pandemic could have necessitated an adverse effect on the management of malaria, resulting in increased deaths. As of 18th April 2023, Africa COVID-19 statistics showed that there have been 8,443,832 cases, 174,211 deaths and 8,269,621 recoveries, while global reports showed approximately, 766 million cases, 7 million deaths, and 659 million recoveries [3]. Meanwhile, WHO malaria cases showed that there are 228 million cases and 405,000 deaths globally in 2018, of which 94% are from Africa [4]. The person-to-person transmission of COVID-19 infection led to the isolation of patients that were administered a variety of treatments at the onset of the outbreak. There are specific and approved antiviral vaccines (e.g., Pfizer, Moderna, Johnson & Johnson etc.) against COVID-19 infection for potential therapy of humans. Nations in sub-Saharan Africa are tasked with protecting their populations from both malaria and the burgeoning COVID-19 epidemic, which accounts for more than 90% of all malaria illnesses and fatalities globally. The growth of medication resistance and the shortage of an effective and secure vaccination have made it more difficult to reduce the severity of malaria. [5]. The COVID-19 pandemic is currently the focus of national health services' action, which is putting further strain on existing overburdened and underfunded healthcare services. [7]. mixed infections of malaria and COVID-19 are likely in nations that have a substantial malaria incidence, where the geographical distribution of both diseases significantly overlaps, according to Gutman et al. [7]. The interconnectedness between malaria and COVID-19 could give rise to a lethal cycle of co-infection, delivering a dual impact in tropical and sub-tropical regions, particularly in low- and middle-income countries where malaria has been historically prevalence. These regions face the double burden of high malaria incidence and the significant effect of COVID-19 on the accessibility of crucial malaria control measures.

Several compartmental models were formulated and utilized in the past to study malaria [8, 9, 11, 12] and COVID-19 [13, 14, 15] transmission dynamics and control. Nevertheless, there is a scarcity of compartmental mathematical models that have been developed and utilized to investigate the transmission and management of co-infection involving malaria and COVID-19.[16, 17]. For example, a joint epidemiological model was developed to examine the simultaneous changing of malaria and COVID-19 [16]. The steadiness of their models was examined to determine the presence of disease-free and endemic equilibrium points.

Additionally,in a separate investigation, researchers constructed and looked at a COVID-19-malaria mixed infection model to explore how threshold level and the dissemination rate of mixed infection influence the synergistic interplay between these two diseases. A bifurcation analysis was performed and the model was found to exhibit a backward bifurcation. The

stability of the COVID-19 sub-model and the malaria sub-model was analysed to determine the presence of no disease equilibrium. They found that the disease-free equilibrium is locally asymptotically stable when the basic reproduction number is less than unity. Moreover, they showed that when the invasion reproduction number exceeds one, COVID-19 can spread within a population where malaria is prevalent. The numerical simulations of their model indicate that, during the endemic equilibrium of COVID-19 and malaria, the prevalence of infections leads to a rise in the burden of COVID-19 while simultaneously reducing the burden of malaria on the population.

To our knowledge, it is the first time to investigate the following research question: Could co-infected humans witness the rapid progression of COVID-19 or malaria and are more likely to bear the brunt of the burden of COVID-19 or malaria, compared to humans who are infected only with malaria or COVID-19?

The rest of this study is organized as follows: Section 2 is devoted to model development. Theoretical results were presented in section 3. Moreover, Numerical results were conducted in section 4 to justify the theoretical findings. Conclusion were presented in section 5.

2. Model development

Based on the existing models [9, 18], we incorporate classes or compartments relevant to the infection with COVID-19 and malaria into a generalized SIR/SAIR-SI model. The human population is divided into twelve classes to capture various scenarios: Susceptible humans to both malaria and COVID-19, (S_h): Represents individuals who are susceptible to both diseases. Asymptomatic humans with COVID-19 only (A_c): Includes individuals who have been infected with COVID-19 but show no symptoms. symptomatic individuals who have both COVID-19 and malaria (I_c): Represents individuals who have contracted COVID-19 and are displaying symptoms. Recovered humans from COVID-19 only (R_c): Includes individuals who have recovered from COVID-19 and are now immune. Infected humans with malaria only (I_m): Represents individuals who are infected with malaria but have not contracted COVID-19. Recovered individuals from malaria (R_m) encompass those who have recuperated from the disease and acquired immunity. Asymptomatic humans with both malaria and COVID-19 (A_{cm}): Represents individuals who are infected with both diseases but show no symptoms. Humans showing symptoms of both COVID-19 and malaria (I_{cm}): Includes individuals who are infected with both diseases and exhibit symptoms. Recovered from COVID-19 but infected with malaria (R_{ci}): Represents individuals who have recovered from COVID-19 but are now infected with malaria. Recovered from malaria but asymptomatic with COVID-19 (R_{ma}): Includes individuals who have recovered from malaria but are now asymptomatic carriers of COVID-19. Recovered from malaria but infected with COVID-19 (R_{mi}): Represents individuals who have recovered from malaria but are now infected with COVID-19. It is assumed that individuals contract either malaria or COVID-19 first or recover from either malaria or COVID-19 first (i.e., $A_{cm} = A_{mc}$, $I_{cm} = I_{mc}$, $R_{cm} = R_{mc}$). The functions λ_{cm} and λ_{mc} represent the rates at which infected humans with COVID-19 get infected with malaria and vice versa. Let N_v be the total mosquito population and N_h be the total human population. Additionally, let β represent the biting rate of mosquitoes. Therefore, the total number of mosquito bites on humans per unit of time is given by $\frac{\beta N_v}{N_h}$. Among these bites, only the proportion $\frac{\beta N_v}{N_h} \times p_{vh} \frac{I_v}{N_v}$ are infected. Here, p_{vh} represents the rate at which a bite from an infected mosquito on a susceptible human will result in a new human infection. Therefore, the mosquito force of infection, denoted as λ_{vh} , is calculated as

Considering that $S_h + A_c + I_c + R_c$ humans are susceptible to malaria, the total number of new human malaria infections can be determined as

$$\lambda_{vh} = \frac{\beta p_{vh} I_v}{N_h}. \quad (2.1)$$

Applying a similar approach to the mosquito classes and taking into account that mosquitoes can contract malaria from individuals co-infected with both COVID-19 and malaria, the rate at which humans infect mosquitoes is given by

$$\lambda_{hv} = \frac{\beta p_{hv} [I_m + A_{cm} + I_{cm} + R_{ci} + \alpha(R_m + R_{cm} + R_{ma} + R_{mi})]}{N_h}, \quad (2.3)$$

Here, p_{hv} represents the rate at which a bite from an infectious human on a susceptible mosquito will lead to a new mosquito infection. As a result, the overall amount of fresh cases of malaria caused by mosquitoes is provided by

$$\lambda_{hv} S_v = \frac{\beta p_{hv} [I_m + A_{cm} + I_{cm} + R_{ci} + \alpha(R_m + R_{cm} + R_{ma} + R_{mi})]}{N_h} S_v. \quad (2.4)$$

The parameter α represents the modification parameter. Within the model, symptomatic (infected humans) individuals, I_m , receive treatment at a rate γ_m . All individuals have a natural mortality rate μ_h , while infectious individuals experience an additional malaria-induced mortality rate δ_m . The mosquito population undergoes SI dynamics, with mosquitoes being born susceptible (S_v) at a rate Λ_v . After biting infectious humans, mosquitoes become infected (I_v) with a probability of p_{hv} . γ_{cm} , γ_{mc} , and δ_{cm} represent the recovery rate of asymptomatic humans from both COVID-19 and malaria, the recovery rate of symptomatic humans from both malaria and COVID-19, and the disease-induced death rates of humans co-infected with both COVID-19 and malaria, respectively.

Next, we will explicitly introduce the impact of COVID-19 on the transmission of malaria pathogen. The biting rate, β , increases during lockdown periods because insecticide-treated bed nets (ITNs) are less available. Humans are protected from mosquito bites by using insecticide-treated bed nets, thereby reducing the probability of malaria transmission. Moreover, besides protecting individuals who sleep under insecticide-treated nets (ITNs), these nets also offer a degree of community-wide protection against malaria. By killing adult mosquitoes, they effectively diminish the overall mosquito population, subsequently reducing the number of mosquitoes available to bite humans [8]. Long-lasting insecticidal nets (LLINs) exhibit high effectiveness upon purchase and when treated with insecticides, but their efficacy diminishes over time. However, even without insecticide treatment, nets still serve to shield humans from mosquitoes, providing a certain level of protection. A widely held assumption is that the effectiveness of insecticide-treated nets (ITNs) remains constant, whereas untreated bed nets provide approximately 50% of the malaria protection that ITNs offer [19]. Other studies suggest that untreated nets provide similar protection [20]. The impact of lockdown measures on malaria transmission should now be explicitly considered. Restrictions on vehicular movements can negatively affect access to antimalarial drugs in pharmacies, particularly for those who can afford them. Hoarding of medicines has been observed during the pandemic, and shortages in supply have made antimalarial drugs unaffordable in some countries. The COVID-19 intervention strategies such as city lockdowns,

movement restrictions, and disruptions in the supply chain have likely disrupted malaria prevention activities, leading to an increase in malaria prevalence and cases. Consequently, the number of malaria-related deaths may also rise. As an example, when the number of COVID-19 cases or hospitalizations rises, the distribution and coverage of insecticide-treated nets (ITNs) may decline due to resource diversion towards COVID-19 efforts. Consequently, this reduction in ITN coverage could alleviate the burden of COVID-19 but potentially worsen the malaria situation. In this scenario, we assume that the treatment and resources for malaria, including ITNs, are limited due to the diversion of resources toward COVID-19. The per capita recovery rates γ_{ac} , γ_{ic} , and γ_m for both COVID-19 and malaria are dependent on treatment, while the efficacy of ITNs coverage b depends on the number of individuals protected from mosquito bites. However, the per capita treatment rates γ_{ac} and γ_{ic} are not constant but decrease as the number of individuals infected with COVID-19 increases. The force of infection for COVID-19 is denoted as

$$\lambda_c = \frac{\beta_a A_c + \beta_i I_c + \beta_{cm1} A_{cm} + \beta_{cm2} I_{cm} + \beta_{ma} R_{ma} + \beta_{mi} R_{mi}}{N_h}, \quad (2.5)$$

where $S_h + I_m + R_m$ represents the number of humans susceptible to COVID-19. The total number of new COVID-19 infections is

$$\lambda_c(S_h + I_m + R_m) = \frac{\beta_a A_c + \beta_i I_c + \beta_{cm1} A_{cm} + \beta_{cm2} I_{cm} + \beta_{ma} R_{ma} + \beta_{mi} R_{mi}}{N_h}(S_h + I_m + R_m). \quad (2.6)$$

It should be noted that $\lambda_1 = (1 - \varepsilon)\lambda_c$ and $\lambda_2 = \varepsilon\lambda_c$. To account for the effects of COVID-19 on malaria dynamics, two instances are considered, involving disruptions in the distribution of ITNs and the treatment of malaria patients. These instances are modeled using the functional forms (b, γ_m), as follows:

$$b(I_c) = \frac{b_0 I_c}{1 + I_c}, \quad (2.7)$$

$$\gamma_m(I_c) = \frac{\gamma_0 I_c}{1 + I_c}, \quad (2.8)$$

The population dynamics of susceptible humans are characterized by the equation:

$$\dot{S}_h = \Lambda_h - (\lambda_c + \lambda_{vh})S_h - \mu_h S_h + \omega_m R_m + \omega_c R_c + \omega_{cm} R_{cm}. \quad (2.9)$$

The population dynamics for individuals infected with COVID-19 only and individuals who have recovered from COVID-19 only are given by the equations:

$$\dot{A}_c = (1 - \varepsilon)\lambda_c S_h - (\mu_h + \gamma_{ac})A_c - \lambda_{vh}A_c, \quad (2.10)$$

$$\dot{I}_c = \varepsilon\lambda_c S_h - (\mu_h + \delta_c + \gamma_{ic})I_c - \lambda_{vh}I_c, \quad (2.11)$$

$$\dot{R}_c = \gamma_{ac}A_c + \gamma_{ic}I_c - (\mu_h + \omega_c)R_c - \lambda_{vh}R_c, \quad (2.12)$$

Likewise, the population dynamics for individuals infected with malaria pathogen only and those who have recovered from malaria infection only are given by the equations:

$$\dot{I}_m = \lambda_{vh}S_h - (\mu_h + \delta_m + \gamma_m)I_m - \lambda_c I_m, \quad (2.13)$$

$$\dot{R}_m = \gamma_m I_m - (\omega_m + \mu_h)R_m - \lambda_c R_m. \quad (2.14)$$

Furthermore, the dynamics for individuals who contract malaria after already being infected with or recovered from COVID-19 are described by the equations:

$$\dot{A}_{cm} = \rho\lambda_{vh}A_c + (1 - \varepsilon)\lambda_cI_m - (\mu_h + \gamma_1)A_{cm}, \quad (2.15)$$

$$\dot{I}_{cm} = (1 - \rho)\lambda_{vh}A_c + \lambda_{vh}I_c + \varepsilon\lambda_cI_m - (\mu_h + \delta_{cm} + \gamma_2)I_{cm}, \quad (2.16)$$

$$\dot{R}_{ci} = \lambda_{vh}R_c - (\mu_h + \gamma_{ci} + \delta_{ci})R_{ci} \quad (2.17)$$

Similarly, the dynamics for individuals who contract COVID-19 after already being infected with or recovered from malaria are described by the equations:

$$\dot{R}_{ma} = (1 - \varepsilon)\lambda_cR_m - (\mu_h + \gamma_3)R_{ma} \quad (2.18)$$

$$\dot{R}_{mi} = \varepsilon\lambda_cR_m - (\mu_h + \gamma_{mi} + \delta_{mi})R_{mi}. \quad (2.19)$$

Therefore, the dynamics of the total human population are described by the equations (2.9)-(2.19). The system of equations governing the dynamics of the susceptible and infected mosquito populations can be represented as follows:

$$\dot{S}_v = \Lambda_v - \lambda_{hv}S_v - \mu_vS_v, \quad (2.20)$$

$$\dot{I}_v = \lambda_{hv}S_v - (\mu_v + \delta_v)I_v, \quad (2.21)$$

Therefore, when we combine subsystems (2.9)-(2.19) and (2.20)-(2.21), we obtain a comprehensive model that describes the interplay of both malaria and COVID-19 within the same population dynamics. The schematic diagram in Figure 1 illustrates this integrated model. The model consists of two hosts: the human host (representing COVID-19 and malaria) depicted by a rectangle with a yellow line, and the vector of malaria transmission (mosquito) represented by a rectangle delimited by dark blue lines.

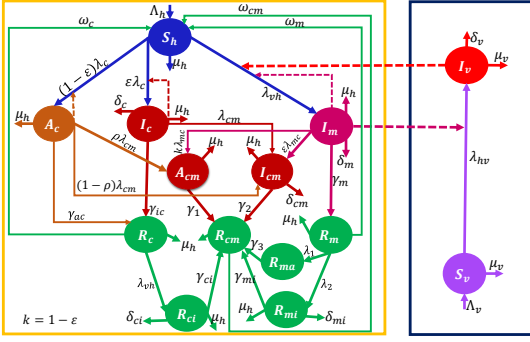


Figure 1: Schematic diagram depicting the joint COVID-19 and malaria model. The model includes two hosts: the human host, represented by a rectangle with a yellow line, which accounts for COVID-19 and malaria, and the vector of malaria transmission (mosquito), represented by a rectangle delimited by dark blue lines. In the human host, individuals who have recovered from malaria (R_m) can be infected by COVID-19 and join the R_{ma} class at a rate $\lambda_1 = (1 - \varepsilon)\lambda_c$, where ε is a proportion representing the likelihood of infection. Another proportion of individuals will join the R_{mi} class at a rate $\lambda_2 = \varepsilon\lambda_c$. Similarly, individuals who have recovered from COVID-19 (R_c) can be infected by malaria and join the R_{ci} class at a certain rate. Among individuals exposed to COVID-19, a proportion ε will exhibit clinical symptoms and join the COVID-19 confirmed class I_c , while the remaining proportion ($k = 1 - \varepsilon$) will become COVID-19 asymptomatic or COVID-19 middle symptomatic individuals (A_c). These transitions occur at a certain rate. Individuals in the COVID-19 confirmed class I_c and those in the COVID-19 asymptomatic or middle symptomatic class A_c recover from SARS-CoV-2 infection at rates γ_{ic} and γ_{ac} , respectively. Individuals confirmed for COVID-19 can also succumb to the virus at a rate δ_c , or they may die naturally at a rate μ_h . Similarly, other compartments in the human host can also experience natural mortality at a rate μ_h . In the vector (mosquito) host, the susceptible vector population increases at a recruitment rate Λ_v and decreases at a rate λ_{hv} due to malaria infection. The vector population also experiences natural mortality at a per capita rate μ_v , as well as disease-induced death at a rate δ_v .

$$\dot{S}_h = \Lambda_h - (\lambda_c + \lambda_{vh})S_h - \mu_h S_h + \omega_m R_m + \omega_c R_c + \omega_{cm} R_{cm}, \quad (2.22)$$

$$\dot{A}_c = (1 - \varepsilon)\lambda_c S_h - (\mu_h + \gamma_{ac})A_c - \lambda_{vh} A_c, \quad (2.23)$$

$$\dot{I}_c = \varepsilon\lambda_c S_h - (\mu_h + \delta_c + \gamma_{ic})I_c - \lambda_{vh} I_c, \quad (2.24)$$

$$\dot{R}_c = \gamma_{ac} A_c + \gamma_{ic} I_c - (\mu_h + \omega_c)R_c - \lambda_{vh} R_c, \quad (2.25)$$

$$\dot{I}_m = \lambda_{vh} S_h - (\mu_h + \delta_m + \gamma_m)I_m - \lambda_c I_m, \quad (2.26)$$

$$\dot{R}_m = \gamma_m I_m - (\omega_m + \mu_h)R_m - \lambda_c R_m, \quad (2.27)$$

$$\dot{R}_{ma} = (1 - \varepsilon)\lambda_c R_m - (\mu_h + \gamma_3)R_{ma} \quad (2.28)$$

$$\dot{R}_{mi} = \varepsilon\lambda_c R_m - (\mu_h + \gamma_{mi} + \delta_{mi})R_{mi} \quad (2.29)$$

$$\dot{A}_{cm} = \rho\lambda_{vh} A_c + (1 - \varepsilon)\lambda_c I_m - (\mu_h + \gamma_1)A_{cm}, \quad (2.30)$$

$$\dot{I}_{cm} = (1 - \rho)\lambda_{vh} A_c + \lambda_{vh} I_c + \varepsilon\lambda_c I_m - (\mu_h + \delta_{cm} + \gamma_2)I_{cm}, \quad (2.31)$$

$$\dot{R}_{cm} = \gamma_1 A_{cm} + \gamma_2 I_{cm} + \gamma_{ci} R_{ci} + \gamma_{mi} R_{mi} + \gamma_3 R_{ma} - \Phi, \quad (2.32)$$

$$\dot{R}_{ci} = \lambda_{vh} R_c - (\mu_h + \gamma_{ci} + \delta_{ci})R_{ci} \quad (2.33)$$

$$\dot{S}_v = \Lambda_v - \lambda_{hv} S_v - \mu_v S_v, \quad (2.34)$$

$$\dot{I}_v = \lambda_{hv} S_v - (\mu_v + \delta_v)I_v. \quad (2.35)$$

where, $\Phi = (\mu_h + \omega_{cm})R_{cm}$

Given the presence of two mono-infection mathematical models for malaria and COVID-19 infections, we have presented sub-models in subsections 2.2 and 2.3. Subsequently, we now provide the generalized findings of the mixed infection model.

2.1. Sub-model of COVID-19 only

To develop the sub-model focused on COVID-19 alone, we set the following initial values: $I_m = R_m = S_v = I_v = R_{ma} = R_{mi} = A_{cm} = I_{cm} = R_{cm} = R_{ci} = 0$. The force of infection for the COVID-19 sub-model is represented by

$$\lambda_{c1} = \frac{\beta_a A_c + \beta_i I_c}{N_h}. \quad (2.36)$$

Therefore, the differential equations for the COVID-19 only are as follows:

$$\dot{S}_h = \Lambda_h N_h - (\lambda_{c1} + \mu_h) S_h + \omega_c R_c, \quad (2.37)$$

$$\dot{A}_c = (1 - \varepsilon)\lambda_{c1}S_h - (\mu_h + \gamma_{ac})A_c, \quad (2.38)$$

$$\dot{I}_c \equiv \varepsilon \lambda_{c1} S_b = (\mu_b + \delta_c + \gamma_{ic}) I_c, \quad (2.39)$$

$$\dot{B}_+ \equiv \gamma_+ A_+ + \gamma_- I_+ = (\mu_+ + \omega_+) B_+ \quad (240)$$

Next, we consider equations (2.37)-(2.40) for the normalized quantities, which allows for convenient analysis of our model in terms of proportions instead of absolute populations. This can be achieved by scaling the population of each class by the aggregate species populations. We introduce the following transformations: $s_h = \frac{S_h}{N_h}$, $a_c = \frac{A_c}{N_h}$, $i_c = \frac{I_c}{N_h}$, $r_c = \frac{R_c}{N_h}$ in the compartments S_h , A_c , I_c , and R_c , respectively. Differentiating these quantities with respect to time t , subject to the restriction $s_h + i_c + r_c = 1$, and using the connections $r_c = 1 - s_h - i_c$ yield:

$$\dot{s}_h = (1 - s_h)\Lambda_h - (\beta_a a_c + \beta_i i_c)s_h + \omega_c(1 - s_h - i_c) + \delta_c s_h i_c, \quad (2.41)$$

$$\dot{a}_c = (1 - \varepsilon)(\beta_a a_c + \beta_i i_c) s_h - (\gamma_{ac} + \Lambda_h) a_c, \quad (2.42)$$

$$\dot{i}_c = \varepsilon(\beta_a a_c + \beta_i i_c) s_h - (\gamma_{ic} + \delta_c + \Lambda_b) i_c + \delta_c i^2, \quad (2.43)$$

These equations hold within the feasible region Ω_c , which denotes the region where the model is both epidemiologically and mathematically meaningful:

$$\Omega_c = \{(s_h, a_c, i_c) \in R_+^3 : 0 \leq s_h, 0 \leq a_c, 0 \leq i_c, s_h + a_c + i_c \leq 1\}$$

Importantly, it should be emphasized that the model remains positively invariant concerning the system (2.41)-(2.43), with \mathbf{R}^3_+ denoting the nonnegative cone of R^3_+ , inclusive of its lower dimensional faces. Moreover, we denote the boundary and interior of Ω_c as $\partial\Omega_c$ and $\dot{\Omega}_c$, respectively.

2.2. Malaria model Only

In this specific case, we can derive the Malaria sub-model by setting the following parameters to zero: $A_c = I_c = R_c = R_{ma} = R_{mi} = A_{cm} = I_{cm} = R_{cm} = R_{ci} = 0$. The mosquito force of infection, which represents the rate at which humans are being infected by mosquitoes, is denoted as

$$\lambda_{vh1} = \frac{\beta p_{vh} I_v}{N_l}$$

Conversely, the rate at which mosquitoes are being infected by humans is given by

$$\lambda_{hv1} = \frac{\beta p_{hv}(I_m + \alpha R_m)}{N_1}.$$

Table 1: Description of variables for the COVID-19 and malaria model.

Definition	Symbols
Susceptible humans to both COVID-19 and malaria	S_h
Infectious humans for malaria	I_m
Asymptomatic humans for COVID-19	A_c
Asymptomatic humans for both COVID-19 and malaria	A_{cm}
Symptomatic humans for COVID-19	$I_c.$
Symptomatic humans for both COVID-19 and malaria	I_{cm}
Recovered humans for COVID-19	R_c
Humans recovered from both COVID-19 and malaria	R_{cm}
Humans recovered from malaria but asymptomatic with COVID-19	R_{ma}
Humans recovered from malaria but symptomatic with COVID-19	R_{mi}
Humans recovered from COVID-19 but infected with malaria	R_{ci}
Recovered humans for malaria	R_m
Susceptible mosquitoes	S_v
Infectious mosquitoes	I_v

Therefore, the differential equations for the Malaria sub-model can be expressed as follows:

$$\dot{S}_h = \Lambda_h N_h - (\lambda_{vh1} - \mu_h) S_h + \omega_m R_m, \quad (2.44)$$

$$\dot{I}_m = \lambda_{vh1} S_h - (\mu_h + \delta_m + \gamma_m) I_m, \quad (2.45)$$

$$\dot{R}_m = \gamma_m I_m - (\omega_m + \mu_h) R_m, \quad (2.46)$$

$$\dot{S}_v = \Lambda_v - \lambda_{hv1} S_v - \mu_v S_v, \quad (2.47)$$

$$\dot{I}_v = \lambda_{hv1} S_v - (\mu_v + \delta_v) I_v \quad (2.48)$$

To facilitate analysis and convenience, we will now consider the normalized quantities of the above equations using a similar approach as in the COVID-19 model. This involves scaling the actual population of each class by the aggregate species populations. We will introduce the following transformations: $s_h = \frac{S_h}{N_h}$, $i_m = \frac{I_m}{N_h}$, $r_m = \frac{R_m}{N_h}$, $s_v = \frac{S_v}{N_v}$, $i_v = \frac{I_v}{N_v}$ in the compartments S_h , I_m , R_m , S_v , I_v and $m = \frac{N_v}{N_h}$ (where m represents the number of mosquitoes per human host). By differentiating these quantities with respect to time t and subject to the condition $s_h + i_m + r_m = 1$, we can derive:

$$\dot{s}_h = \Lambda_h(1 - s_h) - m\beta p_{vh} i_v s_h + \omega_m(1 - s_h - i_m) + \delta_m s_h i_m, \quad (2.49)$$

$$\dot{i}_m = m\beta p_{vh} s_h i_v - (\Lambda_h + \gamma_m + \delta_m) i_m + \delta_m i_m^2, \quad (2.50)$$

$$\dot{i}_v = \beta p_{hv} i_m (1 - i_v) - \Lambda_v i_v \quad (2.51)$$

These equations are defined in Ω_m , where the constructed model makes epidemiological and mathematical meaning:

$$\Omega_m = \{(s_h, i_m, i_v) \in R_+^3 : 0 \leq s_h, 0 \leq i_m, s_h + i_m \leq 1, 0 \leq i_v \leq 1\}$$

The above representation indicates that the model is positively invariant with respect to the system (2.49)-(2.51), where R_+^3 represents the nonnegative cone of R^3 , including its lower-dimensional faces. The boundary and interior of Ω_m are denoted by $\partial\Omega_m$ and Ω_m , respectively.

3. Results

The qualitative investigation of the models, specifically the malaria-only model and the COVID-19 model, aims to analyze the stability and presence of associated equilibria. This

Table 2: Parameter description and values used for the simulations of System.

Symbol	Meaning	Value	Source
p_{vh}	Mosquito to human transmission probability	2.2×10^{-2}	[9]
p_{hv}	Human to mosquito transmission probability	4.8×10^{-2}	[9]
Λ_h	Human birth rate	5.1×10^{-2}	[21]
μ_h	Natural human death rate	0.015	[21]
δ_c	COVID-19 related death	0.026	[22]
δ_m	Malaria related death	9.0×10^{-5}	[9]
γ_m	improvement rate of persons infected with malaria	1.3×10^{-2}	[9]
γ_{ac}	improvement rate of COVID-19 exposed humans	0.11	[10]
γ_{ic}	improvement rate of COVID-19 infected persons	0.057	[22]
ε	Proportion of COVID-19 symptomatic individuals	0.22	[23]
ω_m	Rate at which immune humans lose immunity for malaria	0.25	[24]
ω_c	Rate at which immune humans lose immunity for COVID-19	0.3	[25]
Λ_v	Mosquitoes birth rate	83.3	[9]
μ_v	Mosquito natural death rate (Day^{-1})	3.3×10^{-2}	[26]
β	Mosquito biting rate	2.0×10^{-1}	[9]
b	Initial personal protection or ITN coverage	0.53	[29]
δ_v	Disease induced death rate of mosquitoes	0.00044653	[30]
γ_{ci}	Recovery rate of human who recovered from COVID-19 but infected with malaria	0.057	[22]
ω_{cm}	Rate at which immune human loss immunity for both COVID-19 and malaria	0.3, 0.25	[24, 25]
δ_{ci}	Disease induced death rate of human who recovered from COVID-19 but infected with malaria	9.0×10^{-5}	[9]
δ_{cm}	Disease induced death rate of human co-infected with both COVID-19 and malaria	0.361, 9.0×10^{-5}	[9, 22]
δ_{mi}	Disease induced death rate of human who recovered from malaria but infected with COVID-19	0.361	[22]
γ_{mi}	Recovery rate of human who recovered from malaria but infected with COVID-19	1.3×10^{-2}	[9]
β_a	Transmission probability of symptomatic humans to susceptible human	0.373	[22]
β_i	Transmission probability of symptomatic humans to susceptible human	0.197	[22]
γ_1	improvement rate of exposed persons who are co-infected with both COVID-19 and malaria	0.02	[16]
γ_2	improvement rate of infected persons who are mixed infected with both diseases	0.025	[16]
γ_3	improvement rate of COVID-19 exposed persons who are mixed infected with both diseases	0.025	[16]
ρ	Proportion of COVID-19 exposed persons who are mixed infected with malaria	0.333	[16]
β_{cm1}	Transmission probability of asymptomatic humans co-infected with both diseases and infects susceptible human	0.0203	[16]
β_{cm2}	Transmission probability of symptomatic humans co-infected with both diseases infects and susceptible human	0.5249	[17]
β_{ma}	Prob. transmission of recovered human from malaria but asymptomatic to COVID-19 infects susceptible human	0.002	[17]
β_{mi}	Prob. transmission of recovered human from malaria but symptomatic to COVID-19 infects susceptible human	0.001	[16]
α	Modification parameter	0.5	[16]

examination includes conducting global stability analysis and applying optimal control theory. It is assumed that all parameters involved in the models are non-negative.

3.1. The presence and stability of the equilibrium point for malaria

3.1.1. The stability of the malaria-free equilibrium point at a local level

In the absence of the disease, the malaria model exhibits a stable state known as the malaria-free equilibrium, represented by $\pi^0 = (1, 0, 0)$. To ascertain the steadiness of this equilibrium, Jacobian matrix of equations (2.49)-(2.51) was computed at π^0 . The local stability of the malaria-free equilibrium, π^0 , can be determined by analyzing the signs of the eigenvalues of this Jacobian matrix. The malaria-free equilibrium, π^0 , will be locally stable if all the real parts of its eigenvalues are negative.

$$J_{\pi^0} = \begin{pmatrix} -(\Lambda_h + \omega_m + m\beta p_{vh}i_v^* - \delta_m i_m^*) & -\omega_m + \delta_m s_h^* & -m\beta p_{vh}s_h^* \\ m\beta p_{vh}i_v^* & -(\Lambda_h + \gamma_m + \delta_m) + 2\delta_m i_m^* & m\beta p_{vh}s_h^* \\ 0 & \beta p_{hv}(1 - i_v^*) & -\Lambda_v - \beta p_{hv}i_m^* \end{pmatrix} \quad (3.1)$$

Computing the Jacobian at π^0 yields:

$$J_{\pi^0} = \begin{pmatrix} -(\Lambda_h + \omega_m) & \omega_m + \delta_m & -m\beta p_{vh} \\ 0 & -(\Lambda_h + \gamma_m + \delta_m) & m\beta p_{vh} \\ 0 & \beta P_{hv} & -\Lambda_v \end{pmatrix} \quad (3.2)$$

The spectral radius of the Jacobian matrix are given by:

$$-(\Lambda_h + \omega_m), \frac{-(\Lambda_h + \delta_m + \Lambda_v)^2 - 4(\Lambda_h + \gamma_m + \delta_m)\Lambda_v(1 - \mathcal{R}_{0m})}{2}.$$

Describing,

$$\mathcal{R}_{0m} = \frac{m\beta^2 P_{vh} p_{hv}}{\Lambda_v(\Lambda_h + \gamma_m + \delta_m)}$$

Here, R_{0m} represents the number of humans that one infected mosquito infects and the number of mosquitoes infected by one infected human over their expected infected period, assuming completely susceptible human and mosquito populations. The malaria-free equilibrium, π^0 , is locally stable when $\mathcal{R}_{0m} < 1$.

Theorem 3.1. *Malaria-free equilibrium π^0 is stable (locally) whenever $\mathcal{R}_{0m} < \text{unity}$, but Unstable if $\mathcal{R}_{0m} > \text{unity}$.*

3.2. Global Steadiness of malaria-free equilibrium

Theorem 3.2. *Malaria-free equilibrium π^0 of system (2.49)-(2.51) is globally asymptotically stable in the region Ω_m if $\mathcal{R}_{0m} \leq 1$ and unstable otherwise.*

Proof. Consider the Lyapunov function

$$\mathcal{L} = \beta p_{hv}i_m + (\Lambda_h + \gamma_m + \delta_m)i_v. \quad (3.3)$$

The time derivative of \mathcal{L} along the solutions of the malaria model is given by

$$\dot{\mathcal{L}} = m\beta^2 p_{vh}p_{hv}s_h i_v - \beta p_{hv}i_m(\Lambda_h - \gamma_m - \delta_m i_m) + (\Lambda_h + \gamma_m + \delta_m)(\beta p_{hv}i_m(1 - i_v) - \Lambda_v i_v)$$

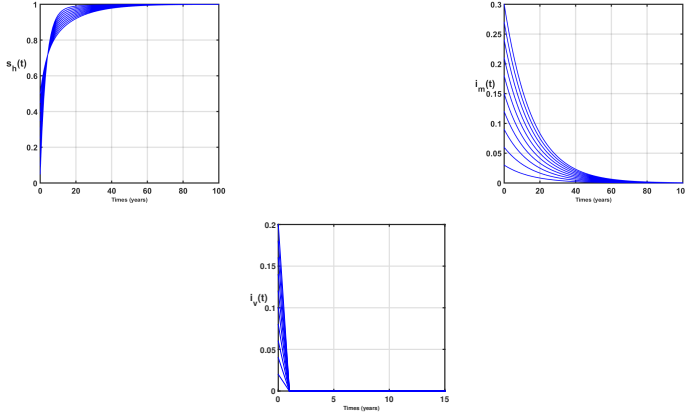


Figure 2: Time-series of variable states of malaria sub-model (2.49)-(2.51) whenever $\mathcal{R}_{0c} < 1$. Parameter values are those of Table 2.

Simplifying further:

$$\begin{aligned}
 &= (\Lambda_h + \gamma_m + \delta_m)\Lambda_v i_v \left[\frac{m\beta^2 p_{vh} p_{hv} s_h}{(\Lambda_h + \gamma_m + \delta_m)\Lambda_v} - 1 \right] + \beta p_{hv} i_m (\delta_m i_m - (\Lambda_h + \gamma_m + \delta_m) i_v) \\
 &= (\Lambda_h + \gamma_m + \delta_m)\Lambda_v i_v (\mathcal{R}_{0m} s_h - 1) - \beta p_{hv} i_m (\Lambda_h + \gamma_m + \delta_m) i_v - \delta_m i_v \\
 &\leq (\Lambda_h + \gamma_m + \delta_m)\Lambda_v i_v (\mathcal{R}_{0m} s_h - 1) \leq 0 \text{ if } \mathcal{R}_{0m} \leq 1
 \end{aligned}$$

Hence, $\dot{\mathcal{L}} \leq 0$ if $\mathcal{R}_{0m} \leq 1$. Moreover, $\dot{\mathcal{L}}$ is zero whenever \mathcal{R}_{0m} is one and when $i_m = i_v = 0$. The biggest compact invariant subset where $\dot{\mathcal{L}} = 0$, denoted as $\{(s_h, i_m, i_v) \in \omega_m | \dot{\mathcal{L}} = 0\}$. On the limit of Ω_m where $i_m = i_v = 0$ (s_h -axis), $\dot{s}_h = (\Lambda_h + \omega_m)(1 - s_h)$, so s_h proceed towards 1 as t proceed towards infinity. Therefore by LaSalle's Theorem, the malaria-free equilibrium point is globally asymptotically stable, completing the proof. This implies that the infected mosquitoes and humans eventually disappear, leading to the elimination of malaria. It is important to observe that threshold number relies on the $m\beta p_{vh}$ and βp_{hv} , as well as the average resident time ($\frac{1}{\Lambda_h + \gamma_m + \delta_m}$) in the ineffective class and the average lifespan ($\frac{1}{\Lambda_v}$) of the mosquitoes. Additionally, \mathcal{R}_{0m} is independent of the loss of immunity rate. Higher values of m and β contribute to the establishment of malaria. These results are depicted in Figure 2 and Figure 3, clearly showing that the malaria-free equilibrium is globally asymptotically stable when $\mathcal{R}_{0m} < 1$, and unstable when $\mathcal{R}_{0m} > 1$. From a biological perspective, controlling malaria involves implementing measures that reduce the malaria reproduction number \mathcal{R}_{0m} below unity. Figure 2: illustrates the time-series depicting the variable states of the malaria sub-model (2.49)-(2.51) in instances where \mathcal{R}_{0c} is less than 1. The parameter values utilized in the simulations correspond to those specified in Table 2. In Figure 3, it can be observed that when $\mathcal{R}_{0m} = 1.9480$, which is greater than 1, the Malaria-free equilibrium loses stability, while the endemic equilibrium point remains stable. Figure 3 illustrates the time-series of variable states in the malaria sub-model (2.49)-(2.51) under the condition where \mathcal{R}_{0m} exceeds 1. The parameter values utilized are the same as those found in Table 2, with the exception of β , which is set to 0.4. Additionally, the values of p_{vh} and p_{hv} are adjusted to 0.8 and 0.65, respectively, resulting in an \mathcal{R}_{0m} value of 1.9480, surpassing 1. \square

Figure 3 illustrates the case $\mathcal{R}_{0m} = 1.9480 > 1$. It clear that the Malaria-free equilibrium becomes unstable and the endemic equilibrium point is stable.

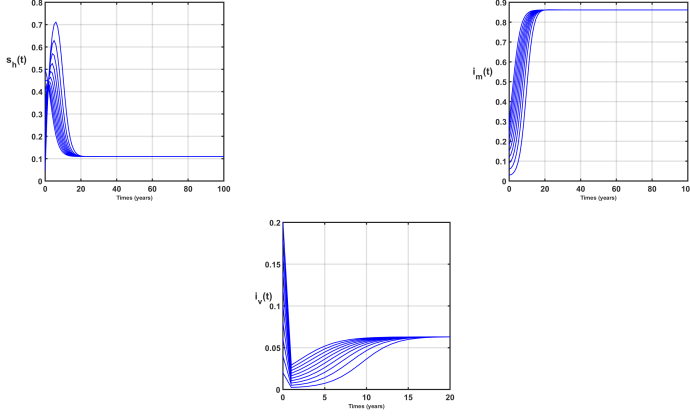


Figure 3: Time-series of variable states of malaria sub-model (2.49)-(2.51) whenever $\mathcal{R}_{0m} > 1$. Parameter values are those of Table 2 except $\beta = 2$, $p_{vh} = 0.8$ and $p_{hv} = 0.65$ such that $\mathcal{R}_{0m} = 1.9480 > 1$.

3.3. Existence and stability of equilibrium for COVID-19

3.3.1. Local stability of COVID-19-free equilibrium

By setting the first derivative and all disease classes to zero, constructed model (2.41)-(2.43) reaches a stable state known as the COVID-19-free equilibrium, denoted as $\varepsilon^0 = (1, 0, 0)$. To assess the steadiness of this equilibrium point, we calculate Jacobian matrix of equations (2.41)-(2.43) at ε^0 . Similar to the approach used for the malaria model, we investigate the local stability of the COVID-19-free equilibrium, ε^0 .

At the stable state of the COVID-19 model (2.41)-(2.43), Jacobian matrix is given by:

$$J_{\varepsilon^0} = \begin{pmatrix} -(\Lambda_h + \omega_c + (\beta_a a_c^* + \beta_i i_c^*) - \delta_c i_c^*) & -\omega_c + \delta_c s_h^* & -\beta_i s_h^* \\ (1 - \varepsilon)(\beta_a a_c^* + \beta_i i_c^*) & -(\gamma_{ac} + \Lambda_h) + (1 - \varepsilon)\beta_a s_h^* & \beta_i(1 - \varepsilon)s_h^* \\ \varepsilon(\beta_a a_c^* + \beta_i i_c^*) & \varepsilon\beta_a s_h^* & \varepsilon\beta_i s_h^* - (\Lambda_h + \gamma_{ic} + \delta_c) + 2\delta_c i_c \end{pmatrix} \quad (3.4)$$

Computing the Jacobian at ε^0 gives:

$$J_{\varepsilon^0} = \begin{pmatrix} -(\Lambda_h + \omega_c) & \omega_c + \delta_c & -\beta_i \\ 0 & -\beta_a(1 - \varepsilon)(\gamma_{ac} + \Lambda_h) & \beta_i(1 - \varepsilon) \\ 0 & \varepsilon\beta_a & -\varepsilon\beta_i - (\Lambda\gamma_{ic} + \delta_c) \end{pmatrix} \quad (3.5)$$

The spectral radius of the Jacobian are given by

$$-(\Lambda_h + \omega_c), \frac{-(\Lambda_h + \delta_c)^2 - 4(\Lambda_h + \gamma_{ac})(\Lambda_h + \gamma_{ic} + \delta_c)(1 - \mathcal{R}_{0c})}{2}.$$

Describing,

$$\mathcal{R}_{0c} = \mathcal{R}_a + \mathcal{R}_i$$

where, $\mathcal{R}_a = \frac{(1-\varepsilon)\beta_a}{\Lambda_h + \gamma_{ac}}$ and $\mathcal{R}_i = \frac{\varepsilon\beta_i}{\Lambda_h + \gamma_{ic} + \delta_c}$

$$\mathcal{R}_{0c} = \frac{(1 - \varepsilon)\beta_a}{\Lambda_h + \gamma_{ac}} + \frac{\varepsilon\beta_i}{\Lambda_h + \gamma_{ic} + \delta_c}$$

Clearly, if the two dominants have negative real parts, then $\mathcal{R}_{0c} < 1$. Thus, we establish the following result Theorem:

Theorem 3.3. *The disease-free (for only COVID-19) equilibrium ε^0 is stable locally whenever $\mathcal{R}_{0c} < \text{one}$ and otherwise if $\mathcal{R}_{0c} > \text{one}$.*

The epidemiological quantity \mathcal{R}_{0c} represents the average number of COVID-19 cases generated by a typical infected individual introduced into an entirely susceptible human population. Furthermore, \mathcal{R}_a describes the number of humans that one asymptomatic human infects over its expected infectious period in a completely susceptible population, while \mathcal{R}_i describes the number of humans that one symptomatic human infects over its expected infected period in a completely susceptible population.

3.4. Global stability of COVID-19 equilibrium

Theorem 3.4. *The COVID-19-free equilibrium $\varepsilon^0 = (1, 0, 0)$ of system (2.41)-(2.43) is globally asymptotically stable in Ω_c if $\mathcal{R}_a, \mathcal{R}_i \leq 1$ and unstable otherwise.*

Proof. Consider the Lyapunov function

$$\mathcal{V} = \beta_a + (\Lambda_h + \gamma_{ac} + \beta_i i_c (\Lambda_h + \gamma_{ic} + \delta_c)) i_c \quad (3.6)$$

The time derivative of (3.6) along the solutions of the COVID-9 model yields:

$$\begin{aligned} \dot{\mathcal{V}} &= \beta_a a_c s_h - (\Lambda_h + \gamma_{ac}) + (\Lambda_h + \gamma_{ic} + \delta_c) \beta_i i_c \\ &= (\Lambda_h + \gamma_{ac}) a_c \left[\frac{(1 - \varepsilon) \beta_a s_h}{\Lambda_h + \gamma_{ac}} - 1 \right] + (\Lambda_h + \gamma_{ic} + \delta_c) i_c \left[\frac{\varepsilon \beta_i s_h}{\Lambda_h + \gamma_{ic} + \delta_c} - 1 \right] - \beta_a a_c (\Lambda_h + \gamma_{ic}) + \beta_i i_c (\delta_c - (\Lambda_h + \gamma_{ic} + \delta_c)) \\ &= (\Lambda_h + \gamma_{ic}) a_c (\mathcal{R}_a s_h - 1) + (\Lambda_h + \gamma_{ic} + \delta_c) i_c (\mathcal{R}_i s_h - 1) \\ &\leq (\Lambda_h + \gamma_{ac}) a_c (\mathcal{R}_a s_h - 1) + (\Lambda_h + \gamma_{ic} + \delta_c) i_c (\mathcal{R}_i s_h - 1) \leq 0 \text{ if } \mathcal{R}_a, \mathcal{R}_i \leq 1 \end{aligned}$$

Hence, $\dot{\mathcal{V}} \leq 0$ if $\mathcal{R}_a, \mathcal{R}_i \leq 1$. Moreover, $\dot{\mathcal{V}}$ is zero whenever $\mathcal{R}_a = \mathcal{R}_i$ is one and when $i_c = a_c = 0$. The biggest compact invariant subset where $\dot{\mathcal{V}} = 0$, denoted as $\{(s_h, i_a, i_c) \in \omega_c | \dot{\mathcal{V}} = 0\}$. On the limit of Ω_c where $i_a = i_c = 0$ (s_h -axis), $\dot{s}_h = (\Lambda_h + \omega_c)(1 - s_h)$, so s_h proceed towards 1 as t proceed towards infinity. Therefore by LaSalle's Theorem, the malaria-free equilibrium point is globally asymptotically stable, completing the proof.

The above results are depicted in Figures 4 and 5. It is evident that the COVID-19-free equilibrium is globally asymptotically stable whenever $\mathcal{R}_{0c} = 1$ and unstable whenever $\mathcal{R}_{0c} > 1$. The biological implication is that controlling COVID-19 requires the implementation of measures to decrease the COVID-19 reproduction number \mathcal{R}_{0c} below unity. \square

The above results are depicted in Figures 4 and 5. It is evident that the COVID-19-free equilibrium is globally asymptotically stable whenever $\mathcal{R}_{0c} = 1$ and unstable whenever $\mathcal{R}_{0c} > 1$. The biological implication is that controlling COVID-19 requires the implementation of measures to decrease the COVID-19 reproduction number \mathcal{R}_{0c} below unity.

Figure 4 illustrates the time-series representation of the variable states of the COVID-19 sub-model (2.41)-(2.43) under the condition where $\mathcal{R}_{0c} < 1$. The parameter values used in this illustration correspond to those provided in Table 2, with the exception of β_a , which is set to 0.135, resulting in an \mathcal{R}_{0c} value of 0.9775, which is less than 1. Figure 5 displays the time-series of variable states for the COVID-19 sub-model (2.41)-(2.43) when \mathcal{R}_{0c} exceeds one. The simulation's parameter values line up with those listed in Table 2. Using these parameter values, we determine that \mathcal{R}_{0c} equals 2.1305, which surpasses the threshold of 1.

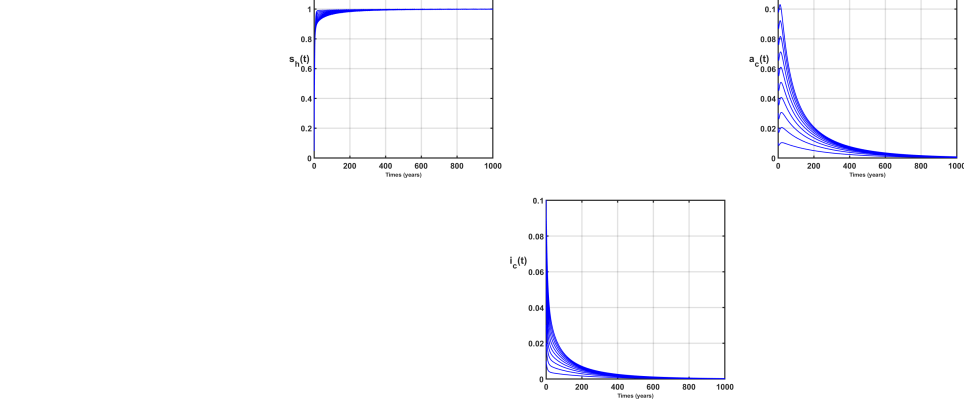


Figure 4: Time-series of variable states of COVID-19 sub-model (2.41)-(2.43) whenever $\mathcal{R}_{0c} < 1$. Parameter values are those of Table 2 except $\beta_a = 0.135$ such that $\mathcal{R}_{0c} = 0.9775 < 1$.

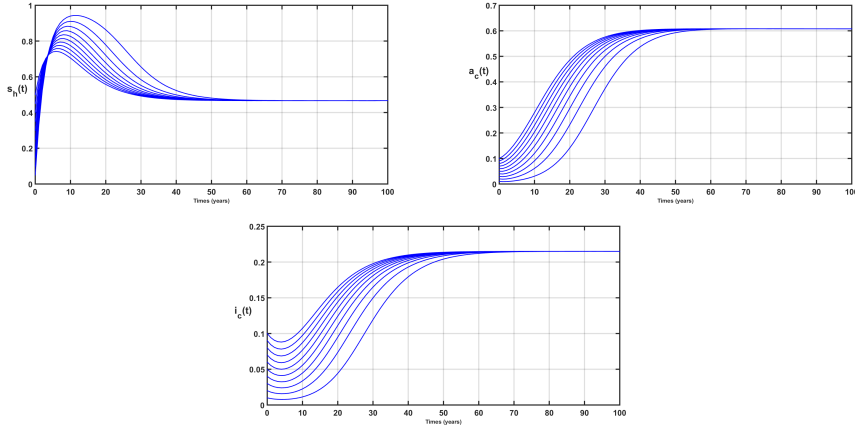


Figure 5: Time-series of variable states of COVID-19 sub-model (2.41)-(2.43) whenever $\mathcal{R}_{0c} > 1$. Parameter values are those of Table 2. With these values, we obtain $\mathcal{R}_{0c} = 2.1305 > 1$.

Figure 5 illustrates the time-series depicting the variable states of the COVID-19 sub-model (2.41)-(2.43) under the condition $\mathcal{R}_{0c} >$ one. The value of the parameters used in the simulations correspond to those in Table 2, which is provided. Based on these parameter values, the calculated \mathcal{R}_{0c} value is 2.1305, which exceeds the threshold of 1.

Figure 5 illustrates the case $\mathcal{R}_{0c} = 2.1305 > 1$. It clear that the Covid-free equilibrium becomes unstable and the endemic equilibrium point is stable.

3.4.1. Impact of COVID-19 on malaria

To examine the interplay between COVID-19 and malaria, we derived a new basic reproduction number for the malaria-COVID-19 populations model (2.22)-(2.35) using actual quantities instead of normalized values (proportions). This approach offers a more comprehensive insight into the effects of COVID-19 on malaria. The basic reproduction number for COVID-19, denoted as \mathcal{R}_c , and the basic reproduction number for malaria, denoted as \mathcal{R}_m are.

$$\mathcal{R}_c = \frac{(1 - \varepsilon)\beta_a}{\mu_h + \gamma_{ac}} + \frac{\varepsilon\beta_i}{\mu_h + \delta_c + \gamma_{ic}} \quad (3.7)$$

and

$$\mathcal{R}_m = \sqrt{\frac{\beta^2 \Lambda_v \mu_h p_{hv} p_{vh} (\alpha \gamma_m + \mu_h + \omega_m)}{\mu_v \Lambda_h (\mu_h + \delta_m + \gamma_m) (\mu_h + \omega_m) (\mu_v + \delta_v)}} \quad (3.8)$$

respectively. The threshold number of the COVID-19-malaria model (2.22)-(2.35), denoted as \mathcal{R}_{mc} is provided as $\mathcal{R}_{mc} = \max\{\mathcal{R}_m, \mathcal{R}_c\}$

To investigate the relationship between \mathcal{R}_c and \mathcal{R}_m , we express \mathcal{R}_c in relation to \mathcal{R}_m and solve for μ_h , yielding equation (3.9).

$$\mu_h = \frac{-(\mathcal{R}_m^2 D_1 - D_2 - D_3) + \sqrt{(\mathcal{R}_m^2 D_1 - D_2 - D_3)^2 - 4(\mathcal{R}_m^2 A - B)D_4 \mathcal{R}_m^2}}{2(\mathcal{R}_m^2 A - B)}$$

where,

$A = \mu_v \Lambda_h (\mu_v + \delta_v)$, $B = \beta^2 \varepsilon_\beta^2 \Lambda_v p_{hv} P_{vh}$, $D_1 = A(\omega_m + D_5)$, $D_2 = B\alpha \gamma_m$, $D_3 = B\omega_m$, $D_4 = AD_5 \omega_m$, $D_5 = \delta_m + \gamma_m$, $D_6 = D_2 + D_3$, and letting

$$\sqrt{(\mathcal{R}_m^2 D_1 - D_6)^2 - 4(\mathcal{R}_m^2 A - B)D_4 \mathcal{R}_m^2} = \mathcal{R}_m^2 D_7 - D_8 - 4\mathcal{R}_m(\mathcal{R}_m D_9 - D_{10}) = \mathcal{R}_m^2 D_7 - D_8 - D_{11} \mathcal{R}_m^2$$

$$\mu_h = \frac{\mathcal{R}_m^2 (D_7 - D_1 - D_{11}) + D_6 - D_8}{2(\mathcal{R}_m^2 A - B)} \quad (3.9)$$

By substituting equation (3.9) into equation (3.7), we obtain the expression for \mathcal{R}_{0c} (equation (3.10)).

$$\mathcal{R}_{0c} = \frac{(1 - \varepsilon) \beta_a (2(\mathcal{R}_m^2 A - B))}{Q + D_6 - D_8 + 2\gamma_{ac}(\mathcal{R}_m^2 A - B)} + \frac{(1 - \varepsilon) \beta_a (2(\mathcal{R}_m^2 A - B))}{Q + D_6 - D_8 + 2(\delta_c + \gamma_{ic})(\mathcal{R}_m^2 A - B)} \quad (3.10)$$

We differentiate \mathcal{R}_c with respect to \mathcal{R}_m , resulting in equation (3.11).

$$\frac{\partial \mathcal{R}_c}{\partial \mathcal{R}_m} = \frac{I_{mc1}(\mathcal{R}_m^2 (D_7 - D_1 - D_{11}) + D_6 - D_8 + 2\gamma_{ac}(\mathcal{R}_m^2 A - B))}{(Q + D_6 - D_8 + 2\gamma_{ac}\mathcal{R}_m^2 A - B)^2} + \frac{I_{mc2}(2Q + 2\delta_c A \mathcal{R}_m + 2\gamma_{ic} A \mathcal{R}_m)}{(Q + D_6 - D_8 + 2\gamma_{ac}(\mathcal{R}_m^2 A - B))^2} \quad (3.11)$$

where, $Q = \mathcal{R}_m^2 (D_7 - D_1 - D_{11})$

$$I_{mc1} = (1 - \varepsilon) \beta_a (4\mathcal{R}_m A) - (1 - \varepsilon) \beta_a (2\mathcal{R}_m^2 A - B) \times 2\mathcal{R}_m^2 (D_7 - D_1 - D_{11}) + \gamma_{ac} (4\mathcal{R}_m^2 A)$$

$$I_{mc2} = \mathcal{R}_m^2 (D_7 - D_1 - D_{11}) + D_6 - D_8 + \delta_c (2\mathcal{R}_m^2 A - B) + \gamma_{ic} (2\mathcal{R}_m^2 A - B) \varepsilon \beta_i (2\mathcal{R}_m^2 A - B)$$

If (3.11) is > 0 , an escalation in malaria occurrences can result in a rise in COVID-19 cases within the community. (3.11) equals zero, it indicates that malaria cases have no substantial impact on the transmission dynamics of COVID-19

Next, we explore the significant effects of COVID-19 on the dynamics of malaria transmission by expressing μ_h in terms of \mathcal{R}_c . This yields equation (3.12), By

$$\mu_h = \frac{-\mathcal{R}_c^2 F_1 + (1 - \varepsilon) \beta_a + \sqrt{(\mathcal{R}_c^2 (F_1^2 + 4(1 - \varepsilon) F_3) - 2(1 - \varepsilon) \beta_a \mathcal{R}_c^2 F_1 + (1 - \varepsilon)^2 \beta_a^2)}}{2\mathcal{R}_c^2} \quad (3.12)$$

where, F_1, F_2, F_3 are intermediate parameters and they define as: $F_1 = \delta_c + \gamma_{ic} + \gamma_{ac}$, $F_2 = \delta_c \gamma_{ac} + \gamma_{ac} \gamma_{ic}$, $F_3 = \delta_c + \gamma_{ic}$. Let

$$\sqrt{\mathcal{R}_c^2 F_1^2 + 4(1 - \varepsilon) F_3} - 2(1 - \varepsilon) \beta_a \mathcal{R}_{0c}^2 F_1 + (1 - \varepsilon)^2 \beta_a^2 = \mathcal{R}_{0c}^2 (F_4 + (1 - \varepsilon)) - 2(1 - \varepsilon) \beta_a$$

$$\mu_h = \frac{\mathcal{R}_c^2 F_1 + (1 - \varepsilon) \beta_a + \mathcal{R}_c^2 (F_4 + 4(1 - \varepsilon)) - 2(1 - \varepsilon) \beta_a}{2\mathcal{R}_c^2}. \quad (3.13)$$

Substituting equation (3.13) into equation (3.8), we obtain the expression for \mathcal{R}_m , (equation (3.14)):

$$\mathcal{R}_m^2 = \frac{B[\alpha\gamma_m + [\mathcal{R}_c(F_4 - F_1) + (1 - \varepsilon) - (1 - \varepsilon)\beta_a]\omega_m]}{\mu_v\Lambda_h(\mu_h + \omega_m)(\mu_v + \delta_v)} \quad (3.14)$$

where, $F_4 = (\mu_h + \gamma_{ac})(\mu_h + \delta_c + \gamma_{ic})$. Differentiating \mathcal{R}_m with respect to \mathcal{R}_c leads to equation (3.15).

$$\frac{\partial \mathcal{R}_m}{\partial \mathcal{R}_c} = \left(\frac{B}{\mu_v\Lambda_h(\mu_h + \omega_m)(\mu_v + \delta_v)} \right)^{\frac{1}{2}} (\alpha\gamma_m + \omega_m(\mathcal{R}_c(F_4 - F_1 + 4(1 - \varepsilon)\beta_a)))^{-\frac{1}{2}} (F_4 - F_1 + 4(1 - \varepsilon))\omega_m. \quad (3.15)$$

if (3.15) is > 0 , an increase in COVID-19 occurrences can lead to a rise in malaria occurrences within the population.

To assess the effect of treating malaria on COVID-19, we partially differentiate \mathcal{R}_m with respect to γ_m , resulting in equation (3.16).

$$\frac{\partial \mathcal{R}_m}{\partial \gamma_m} = - \left(\frac{\beta^2 \varepsilon \beta \Lambda_v \mu_h p_{vh} p_{vh}}{\mu_v \Lambda_h (\mu_h + \omega_m) (\mu_v + \delta_v)} \right)^{\frac{1}{2}} \left(\frac{(\alpha\gamma_m + \mu_h + \omega_m)^{-\frac{1}{2}}}{(\mu_h + \delta_m + \gamma_m)^{-\frac{1}{2}}} \right) \left(\frac{\alpha}{\mu_h + \delta_h + \gamma_m} + \frac{\alpha\gamma_m + \mu_h + \omega_m}{(\mu_h + \delta + \gamma_m)^2} \right) \quad (3.16)$$

Since \mathcal{R}_m is a decreasing function of γ_m , treating COVID-19 positively affects the dynamics of malaria. However, whenever $\mathcal{R}_m > 0$, indicating that \mathcal{R}_m is an increasing function of γ_m , treating COVID-19 negatively affects the dynamics of malaria. Thus, allocating resources from malaria treatment towards COVID-19 could have adverse effects on the human population's survival in terms of malaria.

Figures 6A to 7 illustrate the influence of certain model parameters on the basic reproduction numbers for each sub-model. It is evident that R_c is sensitive to β_a and β_i (Figure 6A), while R_c is sensitive to p_{vh} , p_{hv} , γ_m , and μ_v Figs. 6B, 6C and 6D.

3.4.2. Analysis of optimal control

The effects of control interventions on the infected persons in a mixed infection model of malaria and COVID-19 was examined in this study. This was achieved by applying Maximum Principle developed by Pontryagin to obtain the required conditions for optimizing the control of the model described in equations (2.22)-(2.35). Our approach involved the introduction of multiple time control parameters.

$$\dot{S}_h = \Lambda_h - \lambda_c(1 - u_1)S_h - \lambda_{vh}(1 - u_2)S_h - \mu_h S_h + \omega_m R_m + \omega_c R_c + \omega_{cm} R_{cm}, \quad (3.17)$$

$$\dot{A}_c = (1 - \varepsilon)\lambda_c(1 - u_1)S_h - (\mu_h + \gamma_{ac}u_3)A_c - \lambda_{vh}(1 - u_2)A_c, \quad (3.18)$$

$$\dot{I}_c = \varepsilon\lambda_c(1 - u_1)S_h - (\mu_h + \delta_c + \gamma_{ic}u_3)I_c - \lambda_{vh}(1 - u_2)I_c, \quad (3.19)$$

$$\dot{R}_c = \gamma_{ac}u_3A_c + \gamma_{ic}u_3I_c - (\mu_h + \omega_c)R_c - \lambda_{vh}(1 - u_2)R_c, \quad (3.20)$$

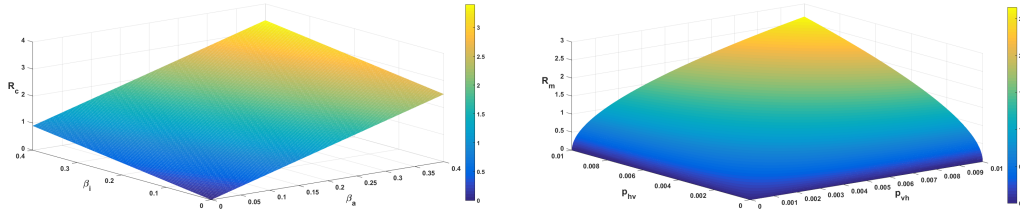
$$\dot{I}_m = \lambda_{vh}(1 - u_2)S_h - (\mu_h + \delta_m + \gamma_m u_4)I_m - \lambda_c(1 - u_1)I_m, \quad (3.21)$$

$$\dot{R}_m = \gamma_m u_4 I_m - (\omega_m + \mu_h)R_m - \lambda_c(1 - u_1)R_m, \quad (3.22)$$

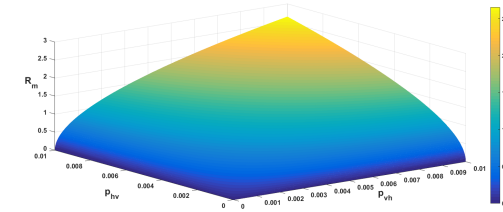
$$\dot{R}_{ma} = (1 - \varepsilon)\lambda_c(1 - u_1)R_m - (\mu_h + \gamma_3 u_5)R_{ma} \quad (3.23)$$

$$\dot{R}_{mi} = \varepsilon\lambda_c(1 - u_1)R_m - (\mu_h + \gamma_{mi}u_4 + \delta_{mi})R_{mi} \quad (3.24)$$

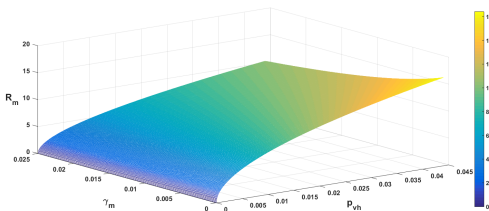
$$\dot{A}_{cm} = \rho\lambda_{vh}(1 - u_2)A_c + (1 - \varepsilon)\lambda_c(1 - u_1)I_m - (\mu_h + \gamma_1 u_5)A_{cm}, \quad (3.25)$$



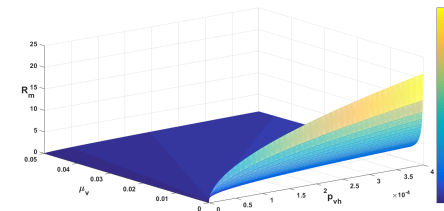
18 (A) 3-D plot of R_c in term of β_a and β_i .



19 (B) 3-D plot of R_m in term of p_{vh} and p_{hv} .

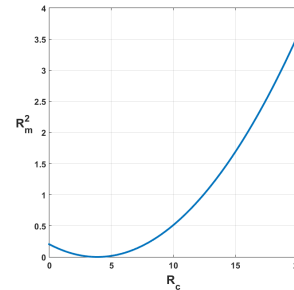


20 (C) 3-D plot of R_m in term of p_{vh} and γ_m .



21 (D) 3-D plot of R_m in term of p_{vh} and μ_v .

22 Figure 6: 3-D plots of the two thresholds R_c and R_m in term of some model parameters.



55 Figure 7: 2-D plot of R_m^2 in term of R_c .

$$\begin{aligned}\dot{I}_{cm} &= (1 - \rho)\lambda_{vh}(1 - u_2)A_c + \lambda_{vh}(1 - u_2)I_c + \varepsilon\lambda_c(1 - u_1)I_m - (\mu_h + \delta_{cm} + \gamma_2 u_5)I_{cm}, \\ \dot{R}_{cm} &= \gamma_1 u_5 A_{cm} + \gamma_2 u_5 I_{cm} + \gamma_{ci} u_3 R_{ci} + \gamma_{mi} u_4 R_{mi} + \gamma_3 u_5 R_{ma} - (\mu_h + \omega_{cm})R_{cm}, \\ \dot{R}_{ci} &= \lambda_{vh}(1 - u_2)R_c - (\mu_h + \gamma_{ci} u_3 + \delta_{ci})R_{ci} \\ \dot{S}_v &= \Lambda_v - \lambda_{hv}(1 - u_2)S_v - \mu_v S_v, \\ \dot{I}_v &= \lambda_{hv}(1 - u_2)S_v - (\mu_v + \delta_v)I_v.\end{aligned}$$

Considering the equations (3.17) to (3.30) mentioned above, the objective functional is taken into account to be:

$$J(u_1, u_2, u_3, u_4, u_5) = \int_0^T [c_1 A_c + c_2 A_{cm} + c_3 I_m + c_4 I_c + c_5 I_{cm} + c_6 I_v + k_1 u_1^2 + k_2 u_2^2 + k_3 u_3^2 + k_4 u_4^2 + k_5 u_5^2] dt.$$

In equation (3.31), the first six components, namely $c_1 A_c, c_2 A_{cm}, c_3 I_m, c_4 I_c, c_5 I_{cm}, c_6 I_v$, represent the cost associated with infections, specifically malaria and COVID-19. The variable T denotes the final time for the treatment strategy, while 0 indicates the initial time when the treatment strategy commenced. The time-dependent controls u_1, u_2, u_3, u_4 , and u_5 are bounded and possess Lebesgue integrable functions. We designate u_1 and u_2 to symbolize the efforts directed towards preventing COVID-19 and malaria infections, respectively. Similarly, u_3 and u_4 represent the control measures for treating COVID-19 and malaria-infected individuals. It is required that $0 \leq u_3 \leq a_1$, where a_1 represents the efficacy of vaccines used in the treatment of COVID-19-infected individuals. Additionally, $0 \leq u_4 \leq a_2$, where a_2 represents the efficacy of drugs used in the treatment of malaria-infected individuals.

Furthermore, we denote u_5 as the control measure for treating individuals co-infected with both diseases. This control function satisfies $0 \leq u_5 \leq a_3$, where a_3 represents the efficacy of drugs used in the treatment of co-infected individuals, as well as the cost associated with administering prevention and treatment measures. The objective is to minimize the values of $(u_1, u_2, u_3, u_4, u_5)$ while subjecting them to the constraints specified in system (3.17)-(3.30). Our objective is to acquire an optimal set of controls, denoted as $u_1^*, u_2^*, u_3^*, u_4^*, u_5^*$, in order to achieve the best possible outcome.

$$J(u_1^*, u_2^*, u_3^*, u_4^*, u_5^*) = \min \{(u_1, u_2, u_3, u_4, u_5) | u_1, u_2, u_3, u_4, u_5 \in \mathcal{U}\},$$

$\mathcal{U}\{(u_1, u_2, u_3, u_4, u_5)\}$ such that u_1, u_2, u_3, u_4, u_5 are measurable with $0 \leq u_1 \leq 1, 0 \leq u_2 \leq 1, 0 \leq u_3 \leq a_1, 0 \leq u_4 \leq a_2$ and $0 \leq u_5 \leq a_3$ for $t \in [0, T]$ is the control set. The Pontryagin et al Maximum Principle provides an optimal control solution that fulfills the necessary conditions. This principle transforms equations (3.17)-(3.30) and (3.31) into a pointwise

minimization problem involving the Hamiltonian H with respect to u_1, u_2, u_3, u_4 and u_5 .

$$\begin{aligned}
H = & c_1 A_c + c_2 A_{cm} + c_3 I_c + c_4 I_m + c_5 I_{cm} + c_6 I_v + k_1 u_1^2 + k_2 u_2^2 + k_3 u_3^2 + k_4 u_4^2 + k_5 u_5^2 \\
& + Q_{S_h} [\Lambda_h - \lambda_c(1 - u_1) S_h - \lambda_{vh}(1 - u_2) S_h - \mu_h S_h + \omega_m R_m + \omega_c R_c + \omega_{cm} R_{cm}] \\
& + Q_{A_c} [(1 - \varepsilon) \lambda_c(1 - u_1) S_h - (\mu_h + \gamma_{ac} u_3) A_c - \lambda_{vh}(1 - u_2) A_c] \\
& + Q_{I_c} [\varepsilon \lambda_c(1 - u_1) S_h - (\mu_h + \delta_c + \gamma_{ic} u_3) I_c - \lambda_{vh}(1 - u_2) I_c] \\
& + Q_{I_m} [\lambda_{vh}(1 - u_2) S_h - (\mu_h + \delta_m + \gamma_m u_4) I_m - \lambda_c(1 - u_1) I_m] \\
& + Q_{A_{cm}} [\rho \lambda_{vh}(1 - u_2) A_c + (1 - \varepsilon) \lambda_c(1 - u_1) I_m - (\mu_h + \gamma_1 u_5) A_{cm}] \\
& + Q_{I_{cm}} [(1 - \rho) \lambda_{vh}(1 - u_2) A_c + \lambda_{vh}(1 - u_2) I_c + \varepsilon \lambda_c(1 - u_1) I_m - (\mu_h + \delta_{cm} + \gamma_2 u_5) I_{cm}] \\
& + Q_{R_c} [\gamma_{ac} u_3 A_c + \gamma_{ic} u_3 I_c - (\mu_h + \omega_c) R_c - \lambda_{vh}(1 - u_2) R_c] \\
& + Q_{R_m} [\gamma_m u_4 I_m - (\omega_m + \mu_h) R_m - \lambda_c(1 - u_1) R_m] \\
& + Q_{R_{ma}} [(1 - \varepsilon) \lambda_c(1 - u_1) R_m - (\mu_h + \gamma_3 u_5) R_{ma}] \\
& + Q_{R_{mi}} [\varepsilon \lambda_c(1 - u_1) R_m - (\mu_h + \gamma_{mi} u_4 + \delta_{mi}) R_{mi}] \\
& + Q_{R_{cm}} [\gamma_1 u_5 A_{cm} + \gamma_2 u_5 I_{cm} + \gamma_{ci} u_3 R_{ci} + \gamma_{mi} u_4 R_{mi} + \gamma_3 u_5 R_{ma} - (\mu_h + \omega_{cm}) R_{cm}] \\
& + Q_{R_{ci}} [\lambda_{vh}(1 - u_2) R_c - (\mu_h + \gamma_{ci} u_3 + \delta_{ci}) R_{ci}] \\
& + Q_{S_v} [\Lambda_v - \lambda_{hv}(1 - u_2) S_v - \mu_v S_v] + Q_{I_v} [\lambda_{hv}(1 - u_2) S_v - (\mu_v + \delta_v) I_v].
\end{aligned} \tag{3.33}$$

Where $Q_{S_h}, Q_{A_c}, Q_{I_c}, Q_{R_c}, Q_{I_m}, Q_{R_m}, Q_{R_{ma}}, Q_{R_{mi}}, Q_{A_{cm}}, Q_{I_{cm}}, Q_{R_{cm}}, Q_{R_{ci}}, Q_{S_v}$ and Q_{I_v} represent the adjoint variables. The system of equations is derived by computing the relevant partial derivative of Hamiltonian (3.33) with respect to the corresponding state variable.

Theorem 3.5. Given the functions $u_1^*, u_2^*, u_3^*, u_4^*, u_5^*$ and solutions $S_h, A_c, I_c, R_c, I_m, R_m, R_{ma}, R_{mi}, A_{cm}, I_{cm}, R_{ci}, S_v, I_v$ of the corresponding state system (3.17)-(3.30) and (3.31) that reduce $J(u_1, u_2, u_3, u_4, u_5)$ over \mathcal{U} . Subsequently, there are related variables. $Q_{S_h}, Q_{A_c}, Q_{I_c}, Q_{R_c}, Q_{I_m}, Q_{R_m}, Q_{R_{ma}}, Q_{R_{mi}}, Q_{A_{cm}}, Q_{I_{cm}}, Q_{R_{cm}}, Q_{R_{ci}}, Q_{S_v}$ and Q_{I_v} satisfying

$$\frac{-dQ_i}{dt} = \frac{\partial H}{\partial i}. \tag{3.34}$$

where $i = S_h, A_c, I_c, R_c, I_m, R_m, R_{ma}, R_{mi}, A_{cm}, I_{cm}, R_{cm}, R_{ci}, S_v, I_v$ and with the transversality conditions

$$\begin{aligned}
Q_{S_h}(T) &= Q_{A_c}(T) = Q_{I_c}(T) = Q_{R_c}(T) = Q_{I_m}(T) = Q_{R_m}(T) = Q_{R_{ma}}(T) = Q_{R_{mi}}(T) = Q_{A_{cm}}(T) \\
&= Q_{I_{cm}}(T) = Q_{R_{cm}}(T) = Q_{R_{ci}}(T) = Q_{S_v}(T) = Q_{I_v}(T) = 0
\end{aligned} \tag{3.35}$$

and

$$u_1^* = \min \left(1, \max \left(0, \frac{(1 - \varepsilon) \lambda_c [S_h Q_{A_c} + I_m Q_{A_{cm}} + R_m Q_{R_{ma}}] + Q_1}{2K_1} \right) \right) \tag{3.36}$$

$$u_2^* = \min \left(1, \max \left(\frac{\lambda_{vh} S_h (Q_{I_m} - Q_{S_h}) + \lambda_{vh} I_c (Q_{I_{cm}} - Q_{I_c}) + \lambda_{vh} R_c (Q_{R_{ci}} - Q_{R_c}) + Q_2}{2K_2} \right) \right) \tag{3.37}$$

$$u_3^* = \min \left(1, \max \left(\frac{\gamma_{ac} (Q_{A_c} - Q_{R_c}) + \gamma_{ic} I_c (Q_{I_c} - Q_{R_c}) + \gamma_{ci} R_{ci} (Q_{R_{ci}} - Q_{R_{cm}})}{2K_3} \right) \right) \tag{3.38}$$

$$u_4^* = \min \left(1, \max \left(\frac{\gamma_m I_m (Q_{I_m} - Q_{R_m}) + \gamma_{mi} R_{mi} (Q_{R_{mi}} - Q_{R_{cm}})}{2K_4} \right) \right) \quad (3.39)$$

$$u_5^* = \min \left(1, \max \left(\frac{\gamma_1 A_{cm} (Q_{A_{cm}} - Q_{R_{cm}}) + \gamma_2 I_{cm} (Q_{I_{cm}} - Q_{R_{cm}}) \gamma_3 Q_{R_{ma}} (Q_{R_{ma}} - Q_{R_{cm}})}{2K_5} \right) \right) \quad (3.40)$$

where, $Q_1 = \varepsilon \lambda_c [S_h Q_{I_c} + I_m Q_{I_{cm}} + R_m Q_{R_m}] - \lambda_c [S_h Q_{S_h} + I_m Q_{I_m} + R_m Q_{R_m}]$, $Q_2 = \lambda_{hv} S_v (Q_{I_v} - Q_{S_v}) + \lambda_{vh} A_c (Q_{A_c} - \rho Q_{A_{cm}}) - (1 - \rho) \lambda_{vh} A_c Q_{I_{cm}}$.

Proof. This was proofed by referring to Corollary 4.1 of Fleming and Rishel [32], we establish the existence of an optimal control. This result is derived from the convexity of the integrand of J with respect to the control variables u_1, u_2, u_3, u_4 , and u_5 .

Additionally, we consider the state solutions' prior constraint as well as the state system's Lipschitz continuity with regard to the state variables. In order to obtain the differential equations that govern the adjoint variables, we differentiate the Hamiltonian function with respect to both the state and control variables. This is done by evaluating the Hamiltonian at the optimal control. As a result, we obtain the adjoint equations, which can be expressed as follows:

$$\begin{aligned} -\dot{Q}_{S_h} &= \mu_h Q_{S_h} + \frac{\lambda_{vh}(1-u_2)(N_h - S_h)(Q_{I_m} - Q_{S_h})}{N_h} + \frac{\lambda_{vh}(1-u_2)I_c(Q_{I_c} - Q_{I_{cm}})}{N_h} \\ &\quad + \frac{\lambda_{vh}(1-u_2)R_c(Q_{R_c} - Q_{R_{ci}})}{N_h} + \frac{k(1-u_1)(N_h - S_h)((1-\varepsilon)Q_{A_c} - \varepsilon Q_{I_c})}{N_h^2} \\ &\quad - \frac{k(1-u_1)I_m((1-\varepsilon)Q_{A_{cm}} + \varepsilon Q_{I_{cm}})}{N_h^2} + \frac{k(1-u_1)R_m((1-\varepsilon)Q_{R_{ma}} - \varepsilon Q_{R_{mi}})}{N_h^2} \\ &\quad + \frac{k(1-u_1)(I_m Q_{I_m} + R_m Q_{R_m})}{N_h^2} - \frac{k(N_h - S_h)(1-u_1)Q_{S_h}}{N_h^2} \\ &\quad - \frac{\lambda_{vh}(1-u_2)A_c(\rho Q_{A_{cm}} + (1-\rho)Q_{I_{cm}})}{N_h} + \frac{\lambda_{vh}(1-u_2)A_c Q_{A_c}}{N_h} \\ &\quad + \frac{q(1-u_2)S_v(Q_{S_v} - Q_{I_v})}{N_h^2}, \end{aligned} \quad (3.41)$$

$$\begin{aligned} -\dot{Q}_{A_c} &= c_1 + \frac{\lambda_{vh}(1-u_2)S_h(Q_{S_h} - Q_{I_m})}{N_h} + \frac{\lambda_{vh}(1-u_2)I_c(Q_{I_c} - Q_{I_{cm}})}{N_h} + \frac{\lambda_{vh}(1-u_2)R_c(Q_{I_{cm}} - Q_{R_{ci}})}{N_h} \\ &\quad + \frac{(1-u_1)S_h(N_h \beta_a - k)(\varepsilon Q_{I_c} - (1-\varepsilon)Q_{A_c})}{N_h^2} + \frac{\lambda_{vh}(1-u_2)(N_h - A_c)(\rho Q_{A_{cm}} - (1-\rho)Q_{I_{cm}})}{N_h} \\ &\quad + \frac{(1-u_1)I_m(N_h \beta_a - k)(\varepsilon Q_{I_{cm}} + (1-\varepsilon)Q_{A_{cm}})}{N_h^2} \\ &\quad - \frac{\lambda_{vh}(1-u_2)(N_h - A_c)Q_{A_c}}{N_h} - \frac{(1-u_1)R_m(N_h \beta_a - k)Q_{R_m}}{N_h^2} - \frac{(1-u_1)S_h(N_h \beta_a - k)Q_{S_h}}{N_h^2} \\ &\quad + \frac{q(1-u_2)S_v(Q_{S_v} - Q_{I_v})}{N_h^2} - (\mu_h + \gamma_{ac}u_3)Q_{A_c}, \end{aligned} \quad (3.42)$$

$$\begin{aligned}
-\dot{Q}_{I_c} = c_3 + & \frac{\lambda_{vh}(1-u_2)S_h(Q_{S_h}-Q_{I_m})}{N_h} + \frac{\lambda_{vh}(1-u_2)I_c(Q_{I_c}-Q_{I_m})}{N_h} + \frac{\lambda_{vh}(1-u_2)R_c(Q_{R_c}-Q_{R_{ci}})}{N_h} \\
& - \frac{\lambda_{vh}(1-u_2)A_c(\rho Q_{A_{cm}}-(1-\rho)Q_{I_{cm}})}{N_h} + \frac{(1-u_1)S_h(N_h\beta_i-k)(Q_{I_c}+Q_{A_c})}{N_h^2} - (\mu_h+\delta_c+\gamma_{ic}u_2)Q_{I_c} \\
& + \frac{(1-u_1)I_m(N_h\beta_i-k)(\varepsilon Q_{I_{cm}}+(1-\varepsilon)Q_{A_{cm}})}{N_h^2} + \frac{(1-u_1)R_m(N_h\beta_i-k)(\varepsilon Q_{R_{mi}}+(1-\varepsilon)Q_{R_{ma}})}{N_h^2} \\
& + \gamma_{ic}u_3Q_{R_c} - \frac{(1-u_1)R_m(N_h\beta_i-k)}{N_h^2} + \frac{\lambda_{vh}(1-u_2)A_cQ_{A_c}}{N_h} - \frac{(1-u_1)(N_h\beta_i-k)(S_hQ_{S_h}-I_mQ_{I_m})}{N_h^2} \\
& + \frac{q(1-u_2)S_v(Q_{S_v}-Q_{I_v})}{N_h^2},
\end{aligned} \tag{3.43}$$

$$\begin{aligned}
-\dot{Q}_{R_c} = \omega_cQ_{S_h} - (\omega_c+\mu_h)Q_{R_c} + & \frac{\lambda_{vh}(1-u_2)S_h(Q_{S_h}-Q_{I_m})}{N_h} + \frac{\lambda_{vh}(1-u_2)I_c(Q_{I_c}-Q_{I_{cm}})}{N_h} \\
& + \frac{\lambda_{vh}(1-u_2)(N_h-R_c)(Q_{R_{ci}}-Q_{R_c})}{N_h} - \frac{k(1-u_1)S_h(\varepsilon Q_{I_c}+(1-\varepsilon)Q_{A_c})}{N_h^2} \\
& - \frac{\lambda_{vh}(1-u_2)A_c(\rho Q_{A_{cm}}+(1-\rho)Q_{I_{cm}})}{N_h} \\
& + \frac{k(1-u_1)R_mQ_{R_m}}{N_h^2} + \frac{q(1-u)S_v(Q_{S_v}-Q_{I_v})}{N_h^2} + \frac{k(1-u_1)(S_hQ_{S_h}+I_mQ_{I_m})}{N_h^2} \\
& - \frac{k(1-u_1)R_m(\varepsilon Q_{R_{mi}}+Q_{R_{ma}})}{N_h^2} - \frac{k(1-u_1)I_m(\varepsilon Q_{I_m}+(1-\varepsilon)Q_{A_{cm}})}{N_h^2} \\
& - \frac{\lambda_{vh}(1-u_2)A_cQ_{A_c}}{N_h},
\end{aligned} \tag{3.44}$$

$$\begin{aligned}
-\dot{Q}_{I_m} = c_4 + & \frac{\lambda_{vh}(1-u_2)S_h(Q_{S_h}-Q_{I_m})}{N_h} + \frac{\lambda_{vh}(1-u_2)I_c(Q_{I_c}-Q_{I_{cm}})}{N_h} + \frac{\lambda_{vh}(1-u_2)R_c(Q_{R_c}-Q_{R_{ci}})}{N_h} \\
& - \frac{\lambda_{vh}(1-u_2)A_c(\rho Q_{A_{cm}}-(1-\rho)Q_{I_{cm}})}{N_h} - \frac{k(1-u_1)S_h(Q_{I_c}-Q_{A_c})}{N_h^2} + \frac{\lambda_{vh}(1-u_2)A_cQ_{A_c}}{N_h} \\
& + \gamma_m u_4 Q_{R_m} - (\mu_h+\delta_m+\gamma_m u_4)Q_{I_m} \\
& + \frac{k(1-u_1)(N_h-I_m)(\varepsilon Q_{I_{cm}}+(1-\varepsilon)Q_{A_{cm}})}{N_h^2} - \frac{k(1-u_1)R_m(\varepsilon Q_{R_{mi}}+(1-\varepsilon)Q_{R_{ma}})}{N_h^2} \\
& + \frac{k(1-u_1)R_mQ_{R_m}}{N_h^2} + \frac{k(1-u_1)(S_hQ_{S_h}+I_mQ_{I_m})}{N_h^2} + \frac{(N_h\beta p_{hv}(1-u_1)S_v-q(1-u_1)S_v)(Q_{I_v}-Q_{S_v})}{N_h^2},
\end{aligned} \tag{3.45}$$

$$\begin{aligned}
-\dot{Q}_{R_m} = & \omega_m Q_{S_h} - (\omega_m + \mu_h) Q_{R_m} + \frac{\lambda_{vh}(1-u_2)S_h(Q_{S_h} - Q_{I_m})}{N_h} - \frac{\lambda_{vh}(1-u_2)A_c(\rho Q_{A_{cm}} + (1-\rho)Q_{I_{cm}})}{N_h} \\
& + \frac{\lambda_{vh}(1-u_2)I_c(Q_{I_c} - Q_{I_{cm}})}{N_h} + \frac{\lambda_{vh}(1-u_2)R_c(Q_{R_c} - Q_{R_{ci}})}{N_h} + \frac{\lambda_{vh}(1-u_2)A_cQ_{A_c}}{N_h} \\
& - \frac{k(1-u_1)I_m((1-\varepsilon)Q_{A_{cm}} + \varepsilon Q_{I_{cm}})}{N_h^2} - \frac{k(1-u_1)S_h((1-\varepsilon)Q_{A_c} + \varepsilon Q_{I_c})}{N_h^2} \\
& + \frac{k(1-u_1)(N_h - R_m)(\varepsilon Q_{R_{ma}} + (1-\varepsilon)Q_{R_{ma}})}{N_h^2} - \frac{k(1-u_1)(N_h - R_m)Q_{R_m}}{N_h^2} \\
& + \frac{k(1-u_1)(S_h Q_{S_h} + Q_{I_m})}{N_h^2} + \frac{N_h \beta \alpha p_{hv}(1-u_2)S_v - q(1-u_2)S_v(Q_{I_v} - Q_{S_v})}{N_h^2},
\end{aligned} \tag{3.46}$$

$$\begin{aligned}
-\dot{Q}_{R_{ma}} = & \gamma_3 u_5 Q_{R_{cm}} - (\mu_h + \gamma_3 u_5) Q_{R_{ma}} - \frac{\lambda_{vh}(1-u_2)S_h(Q_{sh} - Q_{I_m})}{N_h} \\
& - \frac{\lambda_{vh}(1-u_2)A_c(\rho Q_{A_{cm}} + (1-\rho)Q_{I_{cm}})}{N_h} \\
& + \frac{\lambda_{vh}(1-u_2)I_c(Q_{I_c} - Q_{I_{cm}})}{N_h} + \frac{\lambda_{vh}(1-u_2)A_cQ_{A_c}}{N_h} + \frac{(1-u_1)S_h(N_h \beta_{ma} - k)(\varepsilon Q_{I_c} + (1-\varepsilon)Q_{A_c})}{N_h^2} \\
& + \frac{(1-u_1)I_m(N_h \beta_{ma} - k)(\varepsilon Q_{I_{cm}} + (1-\varepsilon)Q_{A_{cm}})}{N_h^2} - \frac{(1-u_1)S_h(N_h \beta_{ma} - k)Q_{S_h}}{N_h^2} \\
& + \frac{(1-u_1)R_m(N_h \beta_{ma} - k)(\varepsilon Q_{R_{mi}} + (1-\varepsilon)Q_{R_{ma}})}{N_h^2} - \frac{(1-u_1)(N_h \beta_{ma} - k)(R_m Q_{R_m} + I_m Q_{I_m})}{N_h^2} \\
& + \frac{N_h \beta p_{hv} \alpha (1-u_2)S_v - q(1-u_2)S_v(Q_{I_v} - Q_{S_v})}{N_h^2},
\end{aligned} \tag{3.47}$$

$$\begin{aligned}
-\dot{Q}_{R_{mi}} = & \frac{\lambda_{vh}(1-u_2)I_c(Q_{I_c} - Q_{I_m})}{N_h} + \frac{\lambda_{vh}(1-u_2)R_c(Q_{R_c} - Q_{R_{ci}})}{N_h} - (\mu_h + \gamma_{mi} u_4 + \delta_m) Q_{R_{mi}} \\
& - \frac{\lambda_{vh}(1-u_2)A_c(Q_{I_{cm}} + Q_{A_{cm}})}{N_h} + \frac{\lambda_{vh}(1-u_2)S_h(Q_{S_h} - Q_{I_m})}{N_h} + \frac{\lambda_{vh}(1-u_2)A_cQ_{A_c}}{N_h} \\
& + \frac{(1-u_1)I_m(N_h \beta_{mi} - k)(\varepsilon Q_{I_{cm}} - (1-\varepsilon)Q_{A_{cm}})}{N_h^2} + \frac{(1-u_1)R_m(N_h \beta_{mi} - k)(\varepsilon Q_{R_{mi}} + (1-\varepsilon)Q_{R_{ma}})}{N_h^2} \\
& + \frac{(1-u_1)S_h(N_h \beta_{mi} - k)(\varepsilon Q_{I_c} + (1-\varepsilon)Q_{A_c})}{N_h^2} - \frac{(1-u_1)R_m(N_h \beta_{mi} - k)Q_{R_m}}{N_h^2} \\
& - \frac{(1-u_1)S_h(N_h \beta_{mi} - k)Q_{S_h}}{N_h^2} + \frac{N_h \beta p_{hv} \alpha (1-u_2)S_v - q(1-u_2)S_v(Q_{I_v} - Q_{S_v})}{N_h^2},
\end{aligned} \tag{3.48}$$

$$\begin{aligned}
-\dot{Q}_{A_{cm}} = & c_2 + \frac{\lambda_{vh}(1-u_2)S_h(Q_{S_h} - Q_{I_m})}{N_h} + \frac{\lambda_{vh}(1-u_2)I_c(Q_{I_c} - Q_{I_{cm}})}{N_h} + \gamma_1 u_5 Q_{R_{cm}} \\
& + \frac{\lambda_{vh}(1-u_2)R_c(Q_{R_c} - Q_{R_{ci}})}{N_h} - \frac{\lambda_{vh}(1-u_2)A_c(\rho Q_{A_{cm}} + (1-\rho)Q_{I_{cm}})}{N_h} \\
& - \frac{(1-u_1)I_m(\varepsilon Q_{I_{cm}} + (1-\varepsilon)Q_{A_{cm}})}{N_h^2} - \frac{(1-u_1)R_m(\varepsilon Q_{R_{mi}} + (1-\varepsilon)Q_{R_{ma}})}{N_h^2} \\
& - \frac{k(1-u_1)S_h(Q_{I_c} + Q_{A_c})}{N_h^2} + \frac{k(1-u_1)(S_h Q_{S_h} + I_m Q_{I_m})}{N_h^2} + \frac{\lambda_{vh}(1-u_2)A_c Q_{A_c}}{N_h} \\
& + \frac{k(1-u_1)R_m Q_{R_m}}{N_h^2} + \frac{q(1-u_2)S_v(Q_{S_v} - Q_{I_v})}{N_h^2},
\end{aligned} \tag{3.49}$$

$$\begin{aligned}
-\dot{Q}_{I_{cm}} = & c_5 + \frac{\lambda_{vh}(1-u_2)S_h(Q_{S_h} - Q_{I_m})}{N_h} + \frac{\lambda_{vh}(1-u_2)I_c(Q_{I_c} - Q_{R_{cm}})}{N_h} + \frac{\lambda_{vh}(1-u_2)R_c(Q_{R_c} - Q_{R_{ci}})}{N_h} \\
& - \frac{\lambda_{vh}(1-u_2)A_c(\rho Q_{A_{cm}} + (1-\rho)Q_{I_{cm}})}{N_h} + \frac{(1-u_1)S_h(N_h \beta_{cm1} - k)(\varepsilon Q_{I_c} + (1-\varepsilon)Q_{A_c})}{N_h^2} \\
& - (\mu_h + \delta_{cm} + \gamma_2 u_5)Q_{I_{cm}} + \frac{(1-u_1)I_m(N_h \beta_{cm1} - k)(\varepsilon Q_{I_{cm}} + (1-\varepsilon)Q_{A_{cm}})}{N_h^2} \\
& + \frac{(1-u_1)R_m(N_h \beta_{cm1} - k)(\varepsilon Q_{R_{mi}} + (1-\varepsilon)Q_{R_{ma}})}{N_h^2} \\
& - \frac{(1-u_1)I_m(N_h \beta_{cm1} - k)(S_h Q_{S_h} + I_m Q_{I_m})}{N_h^2} + \frac{\lambda_{vh}(1-u_2)A_c Q_{A_c}}{N_h} \\
& - \frac{(1-u_1)R_m(N_h \beta_{cm1} - k)Q_{R_m}}{N_h^2} + \frac{N_h \beta p_{hv}(1-u_2)S_v - q(1-u_2)S_v(Q_{I_v} - Q_{S_v})}{N_h^2},
\end{aligned} \tag{3.50}$$

$$\begin{aligned}
-\dot{Q}_{R_{cm}} = & \frac{\lambda_{vh}(1-u_2)S_h(Q_{S_h} - Q_{I_m})}{N_h} + \frac{\lambda_{vh}(1-u_2)R_c(Q_{R_c} - Q_{R_{ci}})}{N_h} + \frac{\lambda_{vh}(1-u_2)I_c(Q_{I_c} - Q_{I_{cm}})}{N_h} \\
& - \frac{\lambda_{vh}(1-u_2)A_c(\rho Q_{A_{cm}} + (1-\rho)Q_{I_{cm}})}{N_h} - \frac{k(1-u_1)I_m(\varepsilon Q_{I_{cm}} + (1-\varepsilon)Q_{A_{cm}})}{N_h^2} \\
& - \frac{k(1-u_1)R_m(\varepsilon Q_{R_{mi}} + (1-\varepsilon)Q_{R_{ma}})}{N_h^2} - \frac{k(1-u_1)S_h(\varepsilon Q_{I_c} + (1-\varepsilon)Q_{A_c})}{N_h^2} \\
& + \frac{k(1-u_1)(I_m Q_{I_m} + R_m Q_{R_m})}{N_h^2} + \frac{\lambda_{vh}(1-u_2)A_c Q_{A_c}}{N_h} \\
& + \omega_{cm} Q_{S_h} - (\mu_h + \omega_{cm})Q_{R_{cm}} + \frac{k(1-u_1)S_h Q_{S_h}}{N_h^2} \\
& + \frac{N_h \beta \alpha p_{hv}(1-u_2)S_v - q(1-u_2)S_v(Q_{I_v} - Q_{S_v})}{N_h^2},
\end{aligned} \tag{3.51}$$

$$\begin{aligned}
-\dot{Q}_{R_{ci}} &= \frac{\lambda_{vh}(1-u_2)S_h(Q_{S_h} - Q_{I_m})}{N_h} + \frac{\lambda_{vh}(1-u_2)R_c(Q_{R_c} - Q_{R_{ci}})}{N_h} + \frac{\lambda_{vh}(1-u_2)I_c(Q_{I_c} - Q_{I_{cm}})}{N_h} \\
&\quad - \frac{\lambda_{vh}(1-u_2)A_c(\rho Q_{A_{cm}} + (1-\rho)Q_{I_{cm}})}{N_h} - \frac{k(1-u_1)I_m(\varepsilon Q_{I_{cm}} + (1-\varepsilon)Q_{A_{cm}})}{N_h^2} \\
&\quad - \frac{k(1-u_1)R_m(\varepsilon Q_{R_{mi}} + (1-\varepsilon)Q_{R_{ma}})}{N_h^2} - \frac{k(1-u_1)S_h(\varepsilon Q_{I_c} + (1-\varepsilon)Q_{A_c})}{N_h^2} + \frac{\lambda_{vh}(1-u_2)A_cQ_{A_c}}{N_h} \\
&\quad + \gamma_{ci}Q_{R_{cm}} - (\mu_h + \gamma_{ci}u_3 + \delta_{ci})Q_{R_{ci}} + \frac{k(1-u_1)(S_hQ_{S_h} - I_mQ_{I_m})}{N_h^2} + \frac{k(1-u_1)R_mQ_{R_m}}{N_h^2} \\
&\quad + \frac{N_h\beta p_{hv}(1-u_2)S_v - q(1-u_2)S_v(Q_{I_v} - Q_{S_v})}{N_h^2},
\end{aligned} \tag{3.52}$$

$$\begin{aligned}
-\dot{Q}_{S_v} &= \frac{q(1-u_2)(Q_{I_v} - Q_{S_v})}{N_h^2} - \mu_vQ_{S_v}, \\
-\dot{Q}_{I_v} &= \frac{\lambda_{vh}(1-u_2)I_c(Q_{I_{cm}} - Q_{I_c})}{N_h} + \frac{\lambda_{vh}(1-u_2)R_c(Q_{R_c} - Q_{R_{ci}})}{N_h} + \frac{\lambda_{vh}(1-u_2)A_c(\rho Q_{A_{cm}} - Q_{I_{cm}})}{N_h} \\
&\quad + \frac{\lambda_{vh}(1-u_2)(S_hQ_{I_m} - A_cQ_{I_c})}{N_h} - \frac{\lambda_{vh}(1-u_2)S_v}{N_h} - (\mu_v + \delta_v)Q_{I_v},
\end{aligned} \tag{3.53}$$

where, $k = \beta_a A_c + \beta_i I_c + \beta_{cm1} I_{cm} + \beta_{ma} R_{ma} + \beta_{mi} R_{mi}$ and $q = \beta p_{hv}[I_m + A_{cm} + I_{cm} + R_{ci} + \alpha(R_m + R_{ma} + R_{cm} + R_{mi})]$ Solving for $u_1^*, u_2^*, u_3^*, u_4^*$ and u_5^* subject to the constraints , the characterization (3.36)-(3.53) can be derived and we have

$$\begin{aligned}
0 &= \frac{\partial H}{\partial u_1} = 2K_1u_1 - (1-\varepsilon)\lambda_c[S_hQ_{A_c} + I_mQ_{A_{cm}} + R_mQ_{R_{ma}}] - \varepsilon\lambda_c[S_hQ_{I_c} + I_mQ_{I_{cm}} + R_mQ_{R_m}] \\
&\quad + \lambda_c[S_hQ_{S_h} + I_mQ_{I_m} + R_mQ_{R_m}], \\
0 &= \frac{\partial H}{\partial u_2} = 2K_2u_2 + \lambda_{vh}S_h(Q_{S_h} - Q_{I_m}) + \lambda_{vh}I_c(Q_{I_c} - Q_{I_{cm}}) + \lambda_{vh}R_c(Q_{R_c} - Q_{R_{ci}}) \\
&\quad + \lambda_{hv}S_v(Q_{S_v} - Q_{I_v}) + \lambda_{vh}A_c(\rho Q_{A_{cm}} - Q_{A_c}) + (1-\rho)\lambda_{vh}A_cQ_{I_{cm}}, \\
0 &= \frac{\partial H}{\partial u_3} = 2K_3u_3 + \gamma_{ac}(Q_{R_c} - Q_{A_c}) + \gamma_{ic}I_c(Q_{R_c} - Q_{I_c}) + \gamma_{ci}R_{ci}(Q_{R_{cm}} - Q_{R_{ci}}), \\
0 &= \frac{\partial H}{\partial u_4} = 2K_4u_4 + \gamma_mI_m(Q_{R_m} - Q_{I_m}) + \gamma_{mi}R_{mi}(Q_{R_{cm}} - Q_{R_{mi}}), \\
0 &= \frac{\partial H}{\partial u_5} = 2K_5u_5 + \gamma_1A_{cm}(Q_{R_{cm}} - Q_{A_{cm}}) + \gamma_2I_{cm}(Q_{R_{cm}} - Q_{I_{cm}})\gamma_3Q_{R_{ma}}(Q_{R_{cm}} - Q_{R_{ma}}).
\end{aligned} \tag{3.54}$$

Hence, we obtain [34]

$$u_1^* = \frac{(1-\varepsilon)\lambda_c[S_hQ_{A_c} + I_mQ_{A_{cm}} + R_mQ_{R_{ma}}] + Q_1}{2K_1}, \tag{3.55}$$

$$u_2^* = \frac{\lambda_{vh}S_h(Q_{I_m} - Q_{S_h}) + \lambda_{vh}I_c(Q_{I_{cm}} - Q_{I_c}) + \lambda_{vh}R_c(Q_{R_{ci}} - Q_{R_c}) + Q_2}{2K_2}, \tag{3.56}$$

$$u_3^* = \frac{\gamma_{ac}(Q_{A_c} - Q_{R_c}) + \gamma_{ic}I_c(Q_{I_c} - Q_{R_c}) + \gamma_{ci}R_{ci}(Q_{R_{ci}} - Q_{R_{cm}})}{2K_3}, \tag{3.57}$$

$$u_4^* = \frac{\gamma_mI_m(Q_{I_m} - Q_{R_m}) + \gamma_{mi}R_{mi}(Q_{R_{mi}} - Q_{R_{cm}})}{2K_4}, \tag{3.58}$$

$$u_5^* = \frac{\gamma_1 A_{cm}(Q_{A_{cm}} - Q_{R_{cm}}) + \gamma_2 I_{cm}(Q_{I_{cm}} - Q_{R_{cm}})\gamma_3 Q_{R_{ma}}(Q_{R_{ma}} - Q_{R_{cm}})}{2K_5}. \quad (3.59)$$

By employing standard control arguments while taking into account the constraints on the controls, we reach the conclusion.

$$\left. \begin{array}{ll} 0 & \text{If } \zeta_i^* \leq 0 \\ \zeta_i^* & \text{If } 0 < \zeta_i^* < 1 \\ 1 & \text{If } \zeta_i^* \geq 1 \end{array} \right\} = u_i^*, \quad (3.60)$$

for $i \in 1, 2, 3, 4, 5$ and where

$$\zeta_1^* = \frac{(1 - \varepsilon)\lambda_c[S_h Q_{A_c} + I_m Q_{A_{cm}} + R_m Q_{R_{ma}}] + Q_1}{2K_1}, \quad (3.61)$$

$$\zeta_2^* = \frac{\lambda_{vh}S_h(Q_{I_m} - Q_{S_h}) + \lambda_{vh}I_c(Q_{I_{cm}} - Q_{I_c}) + \lambda_{vh}R_c(Q_{R_{ci}} - Q_{R_c}) + Q_2}{2K_2}, \quad (3.62)$$

$$\zeta_3^* = \frac{\gamma_{ac}(Q_{A_c} - Q_{R_c}) + \gamma_{ic}I_c(Q_{I_c} - Q_{R_c}) + \gamma_{ci}R_{ci}(Q_{R_{ci}} - Q_{R_{cm}})}{2K_3}, \quad (3.63)$$

$$\zeta_4^* = \frac{\gamma_m I_m(Q_{I_m} - Q_{R_m}) + \gamma_{mi}R_{mi}(Q_{R_{mi}} - Q_{R_{cm}})}{2K_4}, \quad (3.64)$$

$$\zeta_5^* = \frac{\gamma_1 A_{cm}(Q_{A_{cm}} - Q_{R_{cm}}) + \gamma_2 I_{cm}(Q_{I_{cm}} - Q_{R_{cm}})\gamma_3 Q_{R_{ma}}(Q_{R_{ma}} - Q_{R_{cm}})}{2K_5}. \quad (3.65)$$

Then, we investigate the numerical solutions of the optimality system and describe the outcomes of modifying the optimal controls u_1, u_2, u_3, u_4 , and u_5 , as well as the selected parameters and their meanings across numerous situations. \square

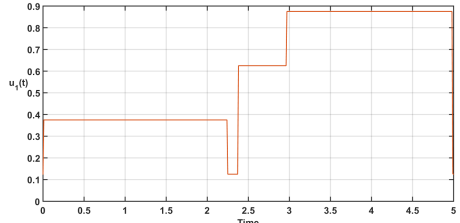
4. Numerical results of the optimal control model

In this report, we present the numerical results of an optimal control model implemented using MATLAB. Table 3. provides a description of various control strategies employed. To obtain the optimal control solutions, we solve the optimality system, which consists of the state system and the adjoint system. The optimality system is solved iteratively using a fourth-order Runge-Kutta scheme. The adjoint equations are solved using a backward fourth-order Runge-Kutta scheme, utilizing the current iteration's solutions of the state equations, due to the transversality condition (3.35). To update the controls, we utilize a convex combination of the previous controls and values derived from the characterizations (3.36)-(3.65). This process is repeated, and we terminate after 315 iterations if the unknowns' values in the previous iterations closely match those in the current iteration. The parameter descriptions and values from Table 2 are employed in the numerical simulations of the co-infection model. We assume $c_i = 1$ for $i = 1, 2, \dots, 6$, and $k_i = 5$ for $i = 1, 2, \dots, 5$. The control profile involves optimizing the objective function J by adjusting the controls (u_1, u_2) for personal protection against malaria and COVID-19, while keeping the remaining controls constant (u_3, u_4 , and u_5) related to malaria and COVID-19 treatment to zero. Similarly, the controls $(u_3, u_4$, and $u_5)$ for malaria treatment, treatment of COVID-19, and infections with both malaria and COVID-19 are utilized to optimize the objective function J , while setting u_1 and u_2 to zero. The control profiles are depicted in Figure 8, illustrating that the optimal protection controls u_1 and u_2 (for malaria and COVID-19, respectively) start at the upper bound before gradually decreasing to the lower bound. Similarly, the optimal treatment controls u_3, u_4 ,

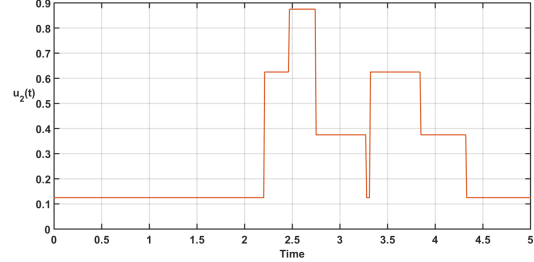
and u_5 (for COVID-19 only, malaria only and mixed infection of both diseases, respectively) also start at the upper bound before gradually decreasing to the lower bound. Finally, to explore the impact of optimal control measures, we analyze the effects of different control strategies on the infected compartments. Figures 9 to 33 display these effects on the infected compartments, providing insights into the effectiveness of the optimal control measures. We examined the prevention of COVID-19 using a single control measure (u_1) and analyzed the time-series of infected compartments (A_{cm} , A_c , I_{cm} , I_c , I_m , and I_v). By focusing on strategy w_1 alone, we aimed to maximize the desire function J , while keeping other controls (u_2 , u_3 , u_4 , and u_5) at zero. Our findings, illustrated in Fig.9, demonstrated a significant reduction in the number of COVID-19-infected humans (A_c , I_c) when control measure u_1 was implemented. However, we also observed an increase in humans co-infected (A_{cm} , I_{cm}). This could be attributed to underlying health conditions or issues such as malaria among COVID-19 infected individuals (see Fig. 9c and 9d). Additionally, the lack of protection against mosquito bites resulted in an increase in the number of infected humans and mosquitoes with malaria (see Fig. 9e and 9f)). To explore the prevention of malaria (u_2), we further analyzed the time-series of infected compartments (A_{cm} , A_c , I_{cm} , I_c , I_m , and I_v) using strategy w_2 alone. Fig.10 revealed similar results as before. Notably, co-infected humans experienced a rapid progression of malaria and bore a significant burden compared to individuals infected solely with COVID-19. We also investigated the effects of treatments (u_3 , u_4 , u_5) for malaria, COVID-19, and co-infection of both diseases. By considering the time-series of infected compartments (A_{cm} , A_c , I_{cm} , I_c , I_m , and I_v) with treatment strategies w_3 , w_4 , and w_5 , we observed similar results in Fig.9 and Fig.10 (see Fig.11, Fig.12, and Fig.13). Furthermore, we explored the combination of two control measures at a time to assess various "what if scenarios." This analysis, incorporating strategies $w_6 - w_{14}$ from Table 3, aimed to understand the impact of optimal control measures on infected compartments (A_{cm} , A_c , I_{cm} , I_c , I_m , and I_v). Fig.14, Fig.15, Fig.16, Fig.17, Fig.18, Fig.19, Fig.20, Fig.21, Fig.22) demonstrated an increase in the number of asymptomatic co-infected humans (A_{cm}), symptomatic co-infected humans (I_{cm}), infected humans with malaria only (I_m), and infected mosquitoes (I_v), while the number of asymptomatic and symptomatic infected individuals with COVID-19 alone decreased for control strategies w_6 , w_7 , w_8 , w_9 , w_{10} , w_{11} , w_{12} , w_{13} , and w_{14} , w_{15} , w_{16} , w_{17} , w_{18} , w_{19} , w_{20} , and w_{21} . Similarly, we analyzed the combination of three control measures at a time, using strategies w_{15} , w_{16} , w_{17} , w_{18} , w_{19} , w_{20} , and w_{21} from Table 3 to optimize the objective function. Compared to combining two control measures, this approach resulted in a slight decrease in the number of infected compartments A_{cm} , I_{cm} , I_m , and I_v . Notably, the number of humans infected with COVID-19 (asymptomatic and symptomatic) decreased significantly (see Fig.23, Fig.24, Fig.25, Fig.26, Fig.27, Fig.28, Fig.29). We further investigated the effects of combining four control measures at a time for various "what if scenarios." This analysis aimed to determine whether a significant reduction in the number of infected compartments A_{cm} , I_{cm} , I_m , and I_v could be achieved. Fig.30, Fig.31, Fig.32 revealed that combining four control measures at a time resulted in a better reduction compared to using three control measures. Finally, we considered the combination of all control measures (u_1 , u_2 , u_3 , u_4 , and u_5) to optimize the objective function J . Fig.33a, Fig.33c, Fig.33e, and Fig.33f illustrated the results, showing a decrease in the number of asymptomatic co-infected humans (A_{cm}), symptomatic co-infected humans (I_{cm}), infected humans with malaria only (I_m), and infected mosquitoes (I_v). However, there was an increase in the number of asymptomatic and symptomatic individuals infected with COVID-19 only. This outcome may be attributed to delays in treatment, vaccination, and other non-pharmaceutical interventions (NPIs).

Table 3: List and description of the control strategies.

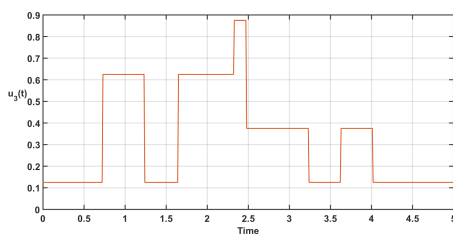
Control strategy	Description	Control strategy	Description
w_0	No control	w_{13}	$u_3 \neq 0, u_4 \neq 0$
w_1	$u_1 \neq 0$	w_{14}	$u_3 \neq 0, u_5 \neq 0$
w_2	$u_2 \neq 0$	w_{15}	$u_1 \neq 0, u_2 \neq 0, u_3 \neq 0$
w_3	$u_3 \neq 0$	w_{16}	$u_1 \neq 0, u_2 \neq 0, u_4 \neq 0$
w_4	$u_4 \neq 0$	w_{17}	$u_1 \neq 0, u_2 \neq 0, u_5 \neq 0$
w_5	$u_5 \neq 0$	w_{18}	$u_1 \neq 0, u_3 \neq 0, u_4 \neq 0$
w_6	$u_1 \neq 0, u_2 \neq 0$	w_{19}	$u_1 \neq 0, u_3 \neq 0, u_5 \neq 0$
w_7	$u_1 \neq 0, u_3 \neq 0$	w_{20}	$u_2 \neq 0, u_3 \neq 0, u_4 \neq 0$
w_8	$u_1 \neq 0, u_4 \neq 0$	w_{21}	$u_2 \neq 0, u_3 \neq 0, u_5 \neq 0$
w_9	$u_1 \neq 0, u_5 \neq 0$	w_{22}	$u_1 \neq 0, u_2 \neq 0, u_3 \neq 0, u_4 \neq 0$
w_{10}	$u_2 \neq 0, u_3 \neq 0$	w_{23}	$u_1 \neq 0, u_2 \neq 0, u_3 \neq 0, u_5 \neq 0$
w_{11}	$u_2 \neq 0, u_4 \neq 0$	w_{24}	$u_2 \neq 0, u_3 \neq 0, u_4 \neq 0, u_5 \neq 0$
w_{12}	$u_2 \neq 0, u_5 \neq 0$	w_{25}	$u_1 \neq 0, u_2 \neq 0, u_3 \neq 0, u_4 \neq 0, u_5 \neq 0$



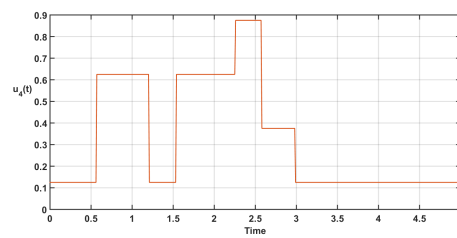
(A) Prevention of COVID-19 infection



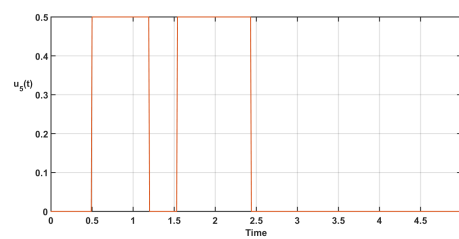
(B) Prevention of malaria infection



(C) COVID-19 treatment



(D) Malaria treatment



(E) Co-infected treatment

Figure 8: Control profiles.

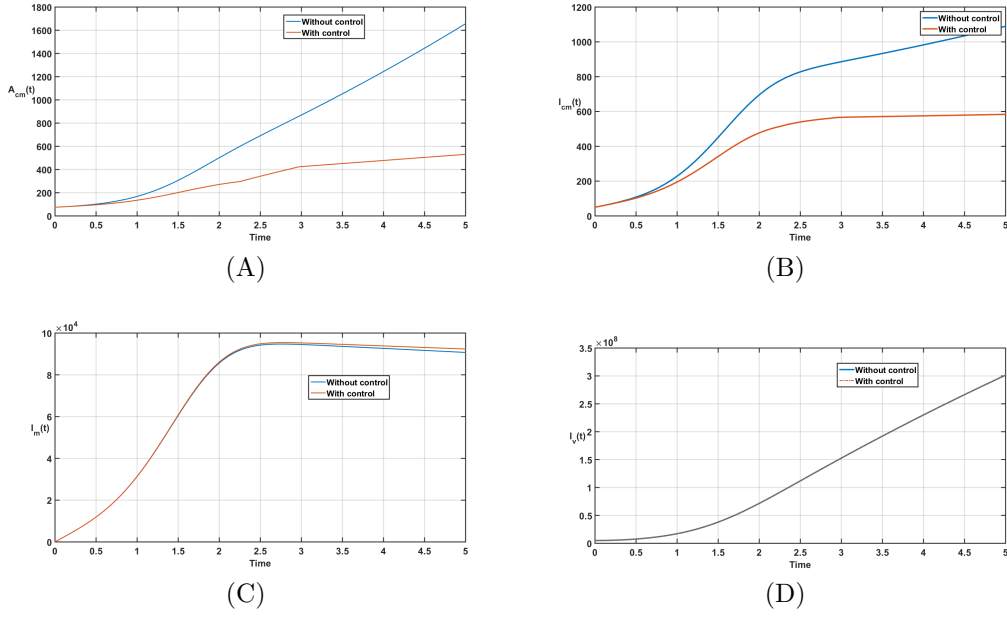


Figure 9: The time-series of infected compartments when the strategy w_1 is used only.

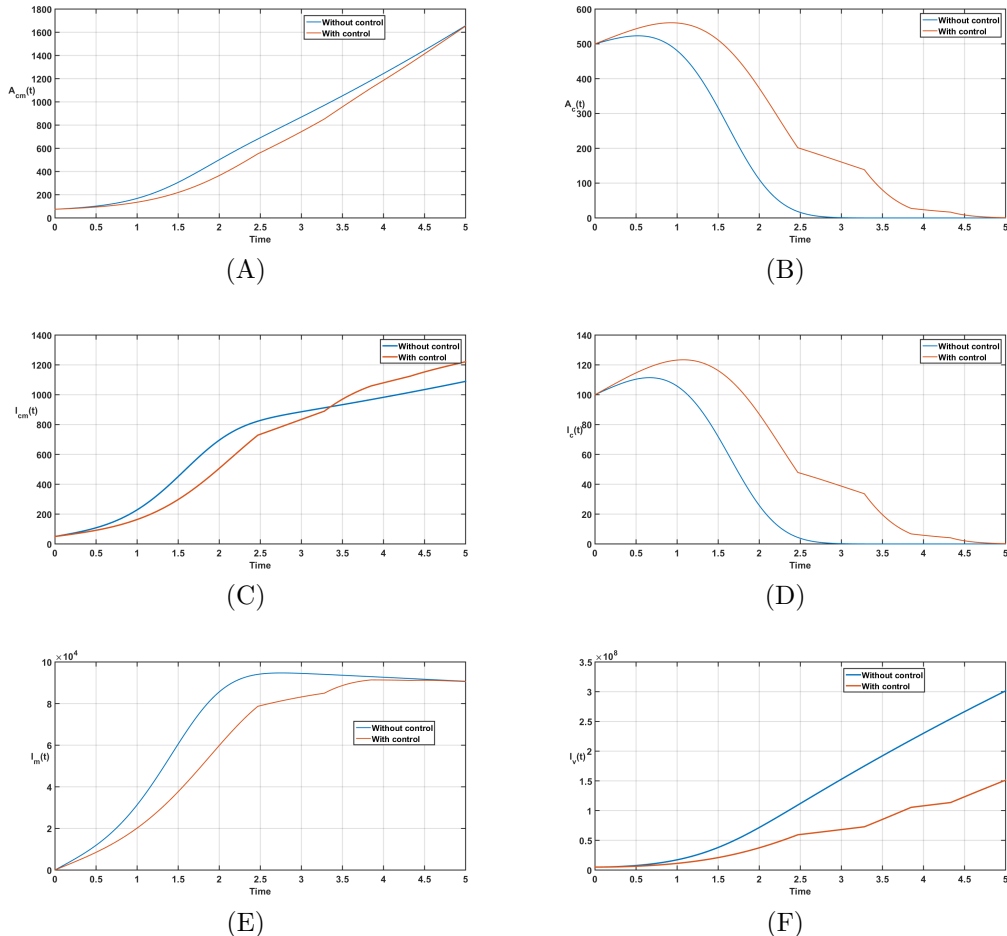


Figure 10: The time-series of infected compartments when the strategy w_2 is used only.

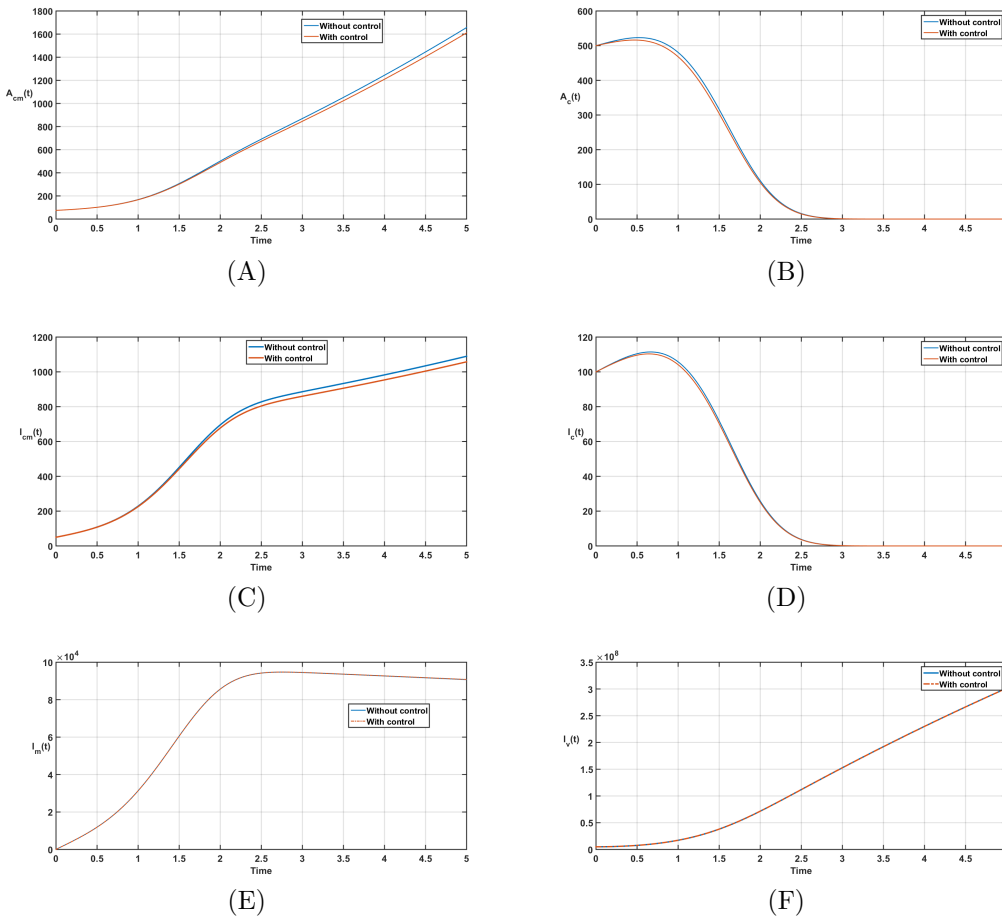


Figure 11: The time-series of infected compartments when the strategy w_3 is used only.

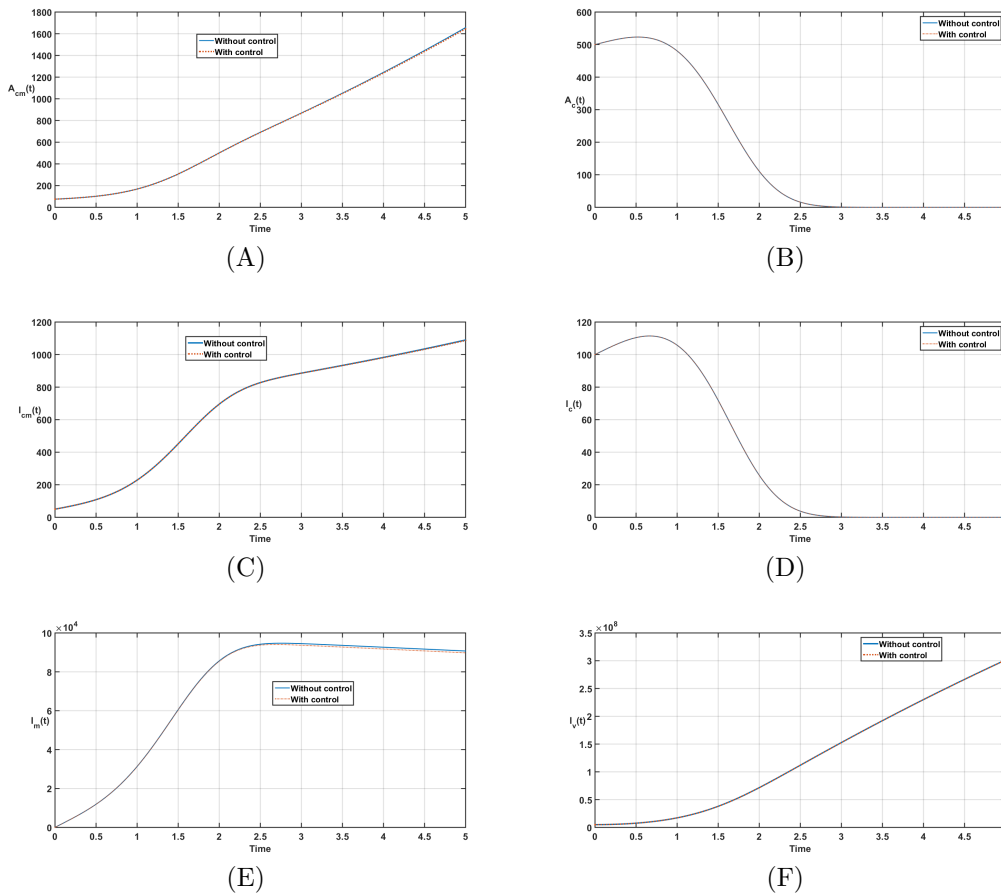


Figure 12: The time-series of infected compartments when the strategy w_4 is used only.

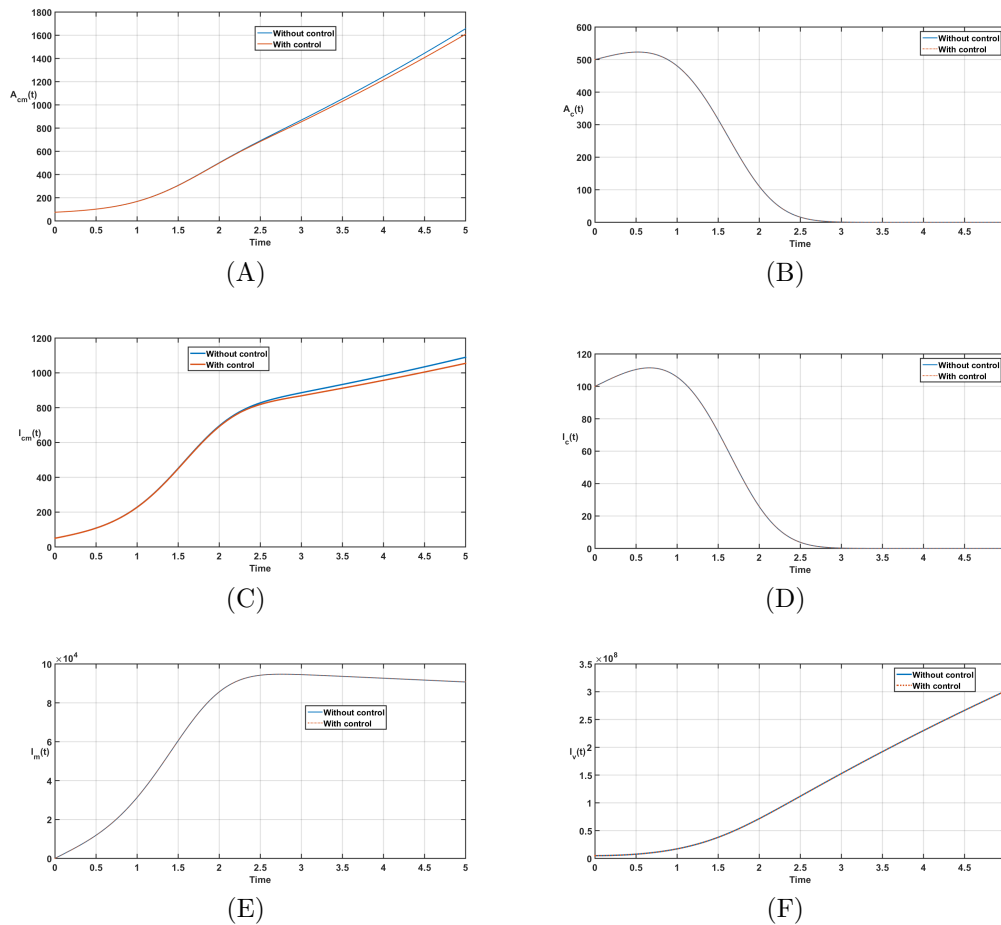


Figure 13: The time-series of infected compartments when the strategy w_5 is used only.

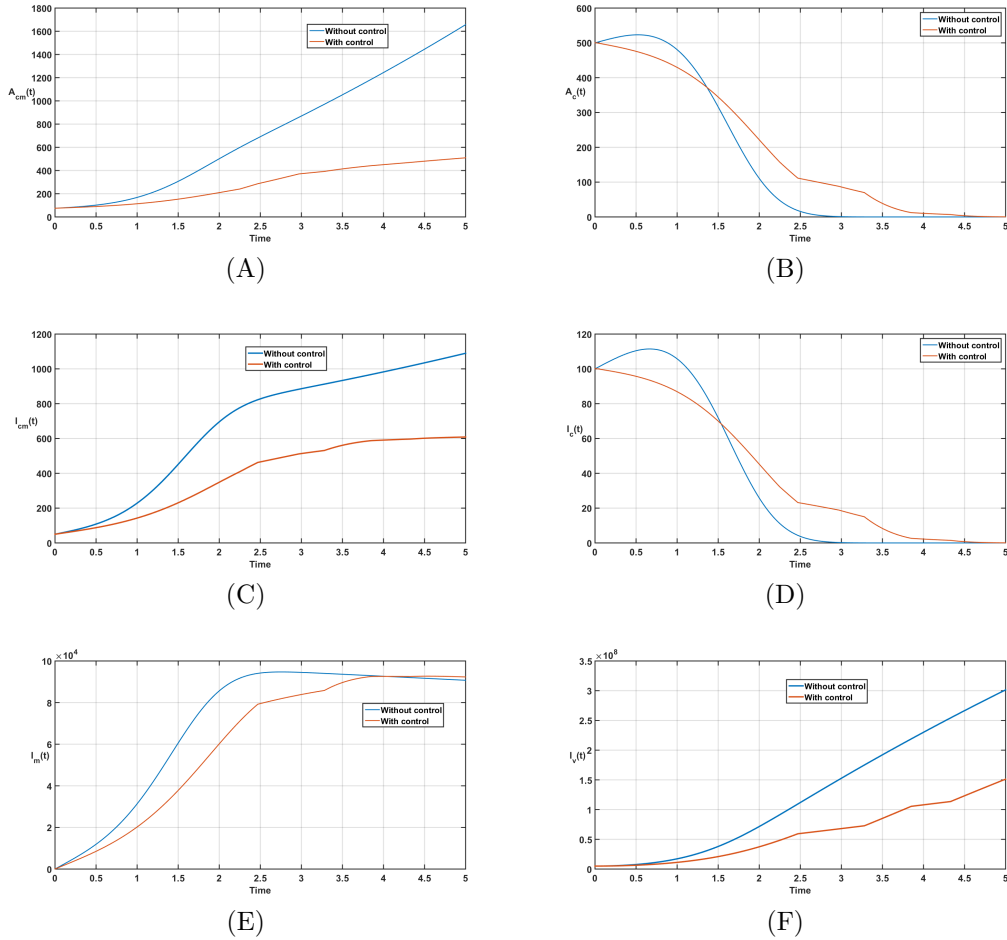


Figure 14: The time-series of infected compartments when the strategy w_6 is used only.

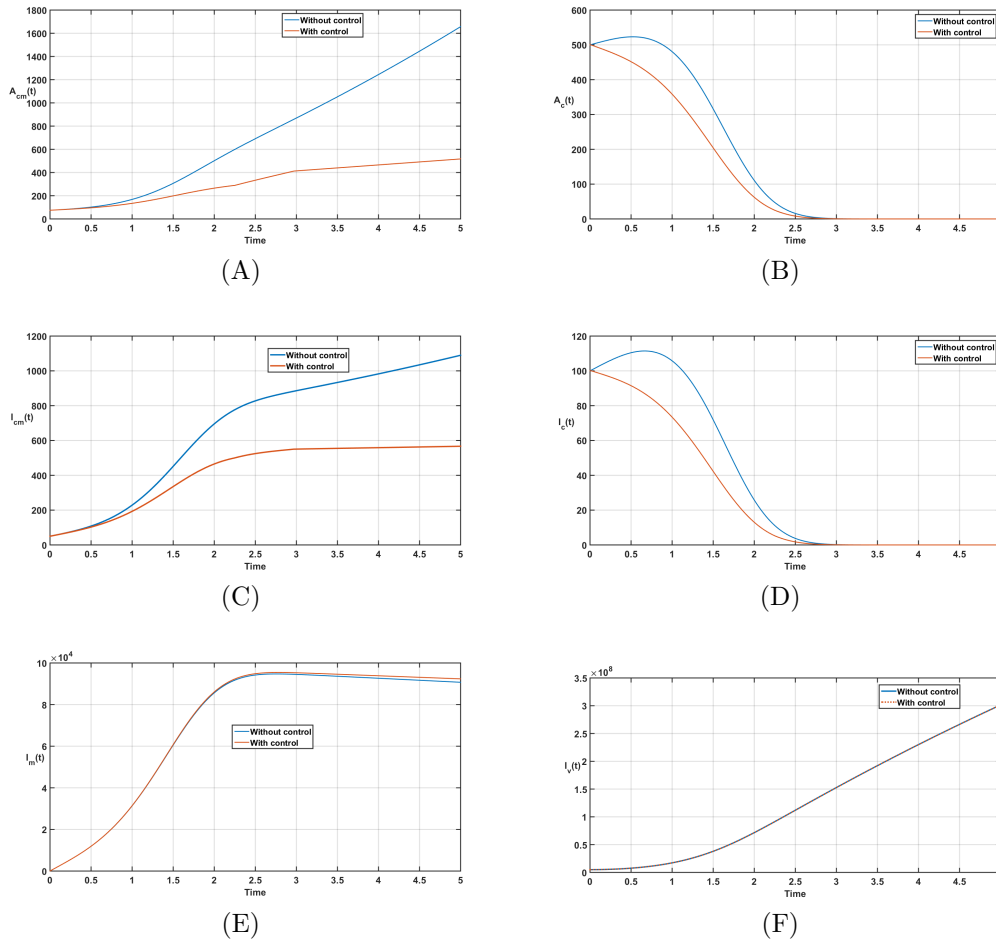


Figure 15: The time-series of infected compartments when the strategy w_7 is used only.

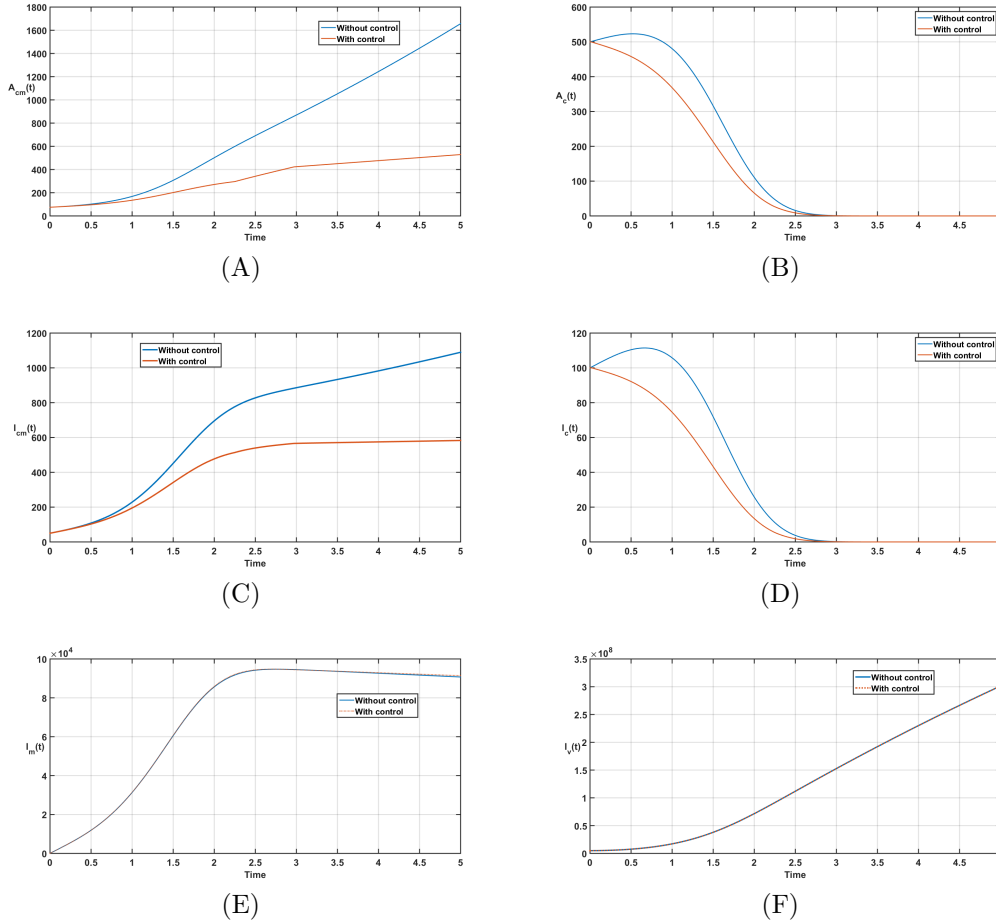
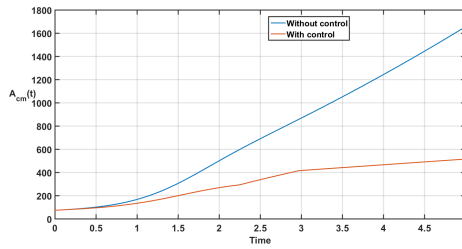
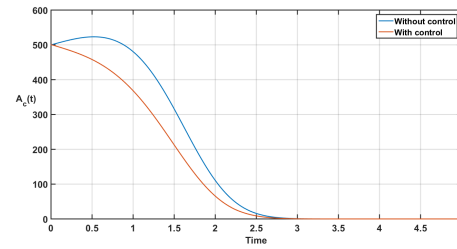


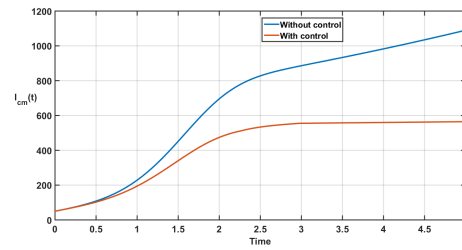
Figure 16: The time-series of infected compartments when the strategy w_8 is used only.



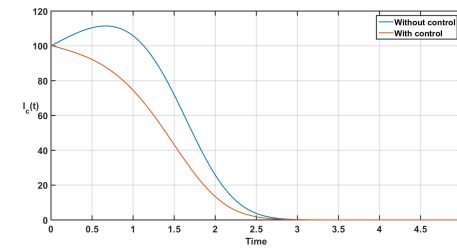
(A)



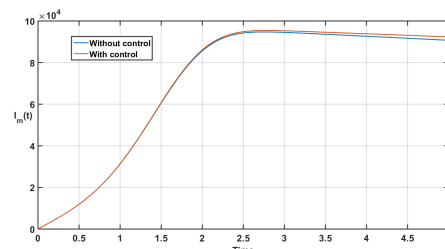
(B)



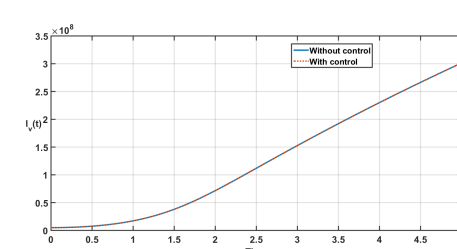
(C)



(D)



(E)



(F)

Figure 17: The time-series of infected compartments when the strategy w_9 is used only.

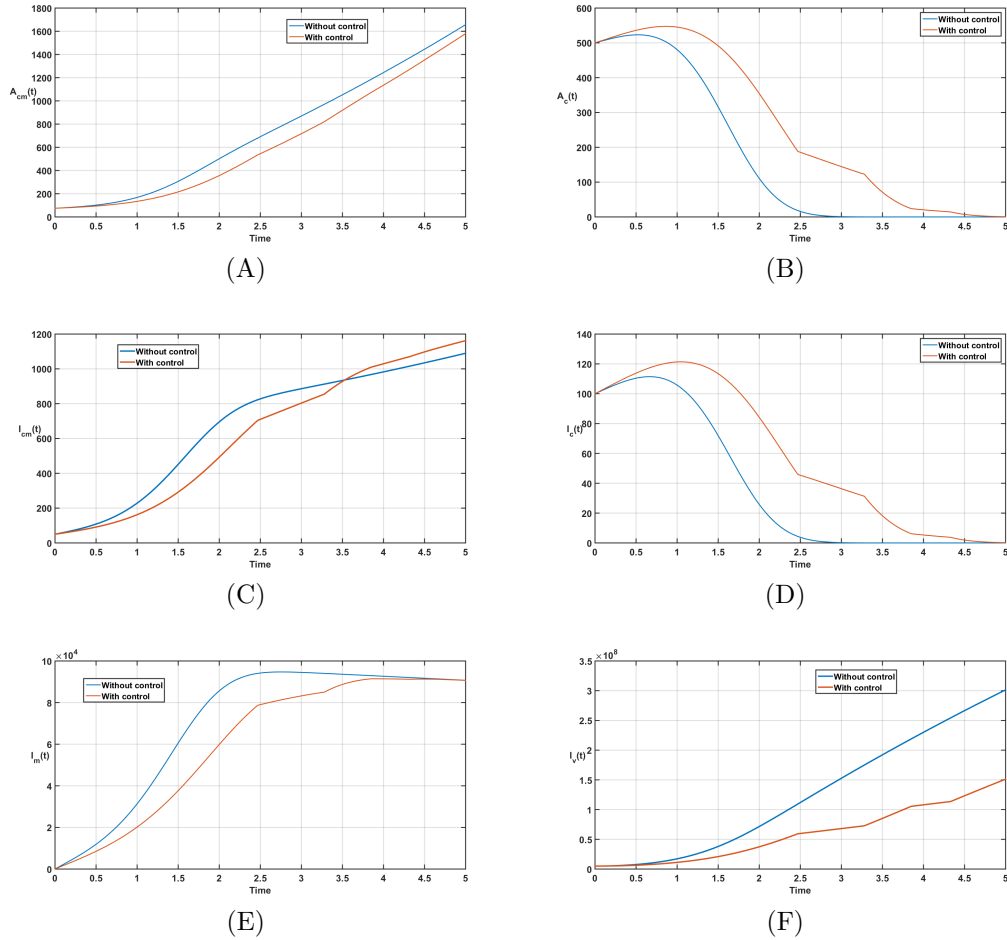


Figure 18: The time-series of infected compartments when the strategy w_{10} is used only.

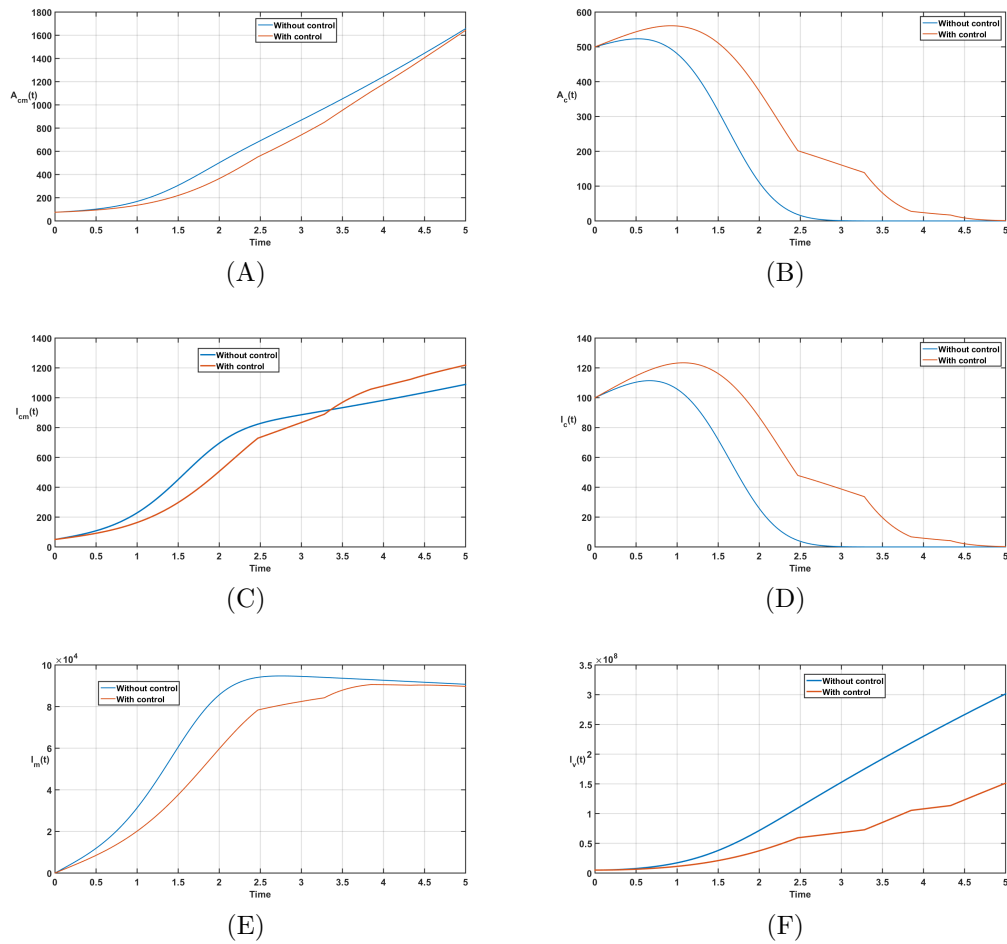


Figure 19: The time-series of infected compartments when the strategy w_{11} is used only.

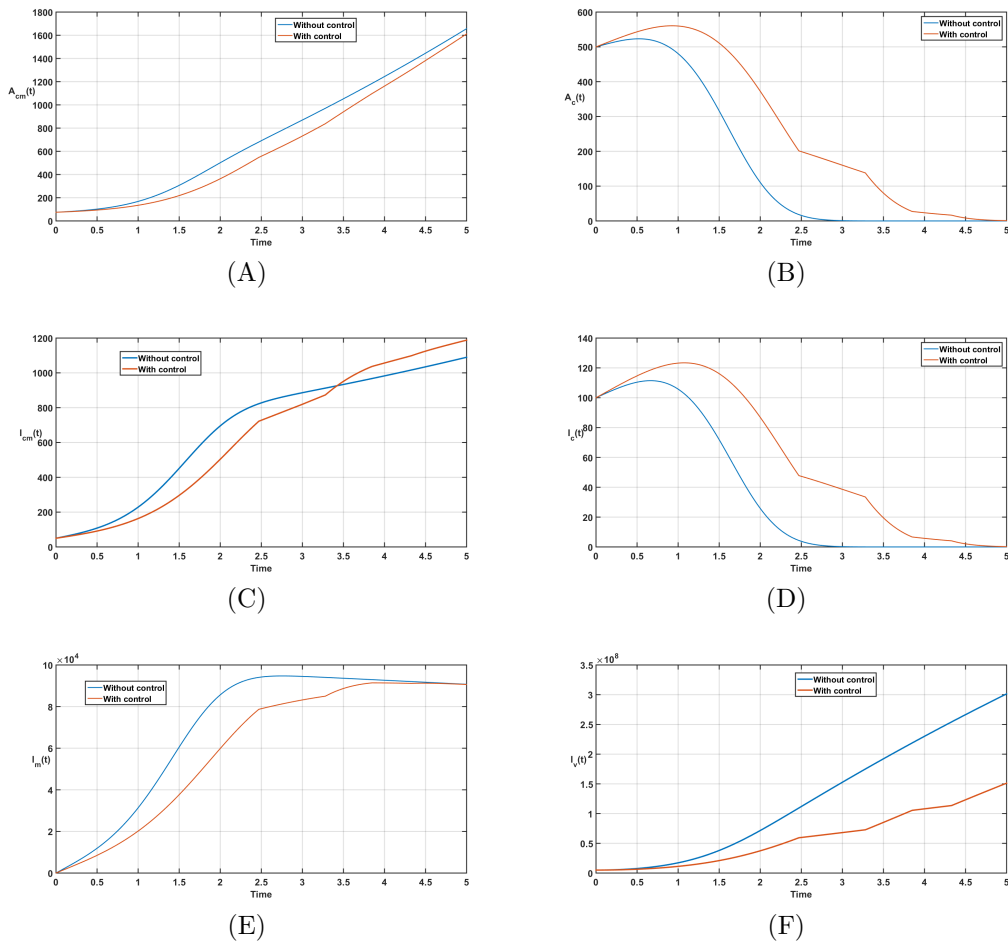


Figure 20: The time-series of infected compartments when the strategy w_{12} is used only.

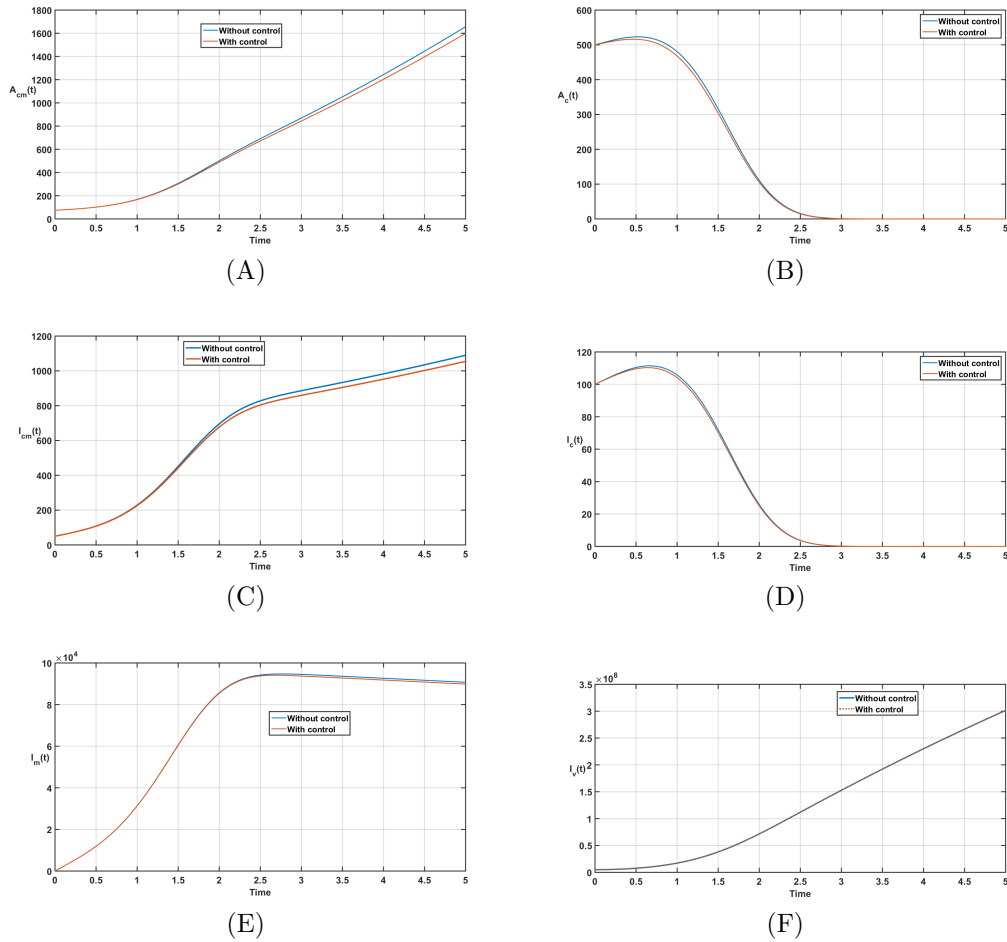


Figure 21: The time-series of infected compartments when the strategy w_{13} is used only.

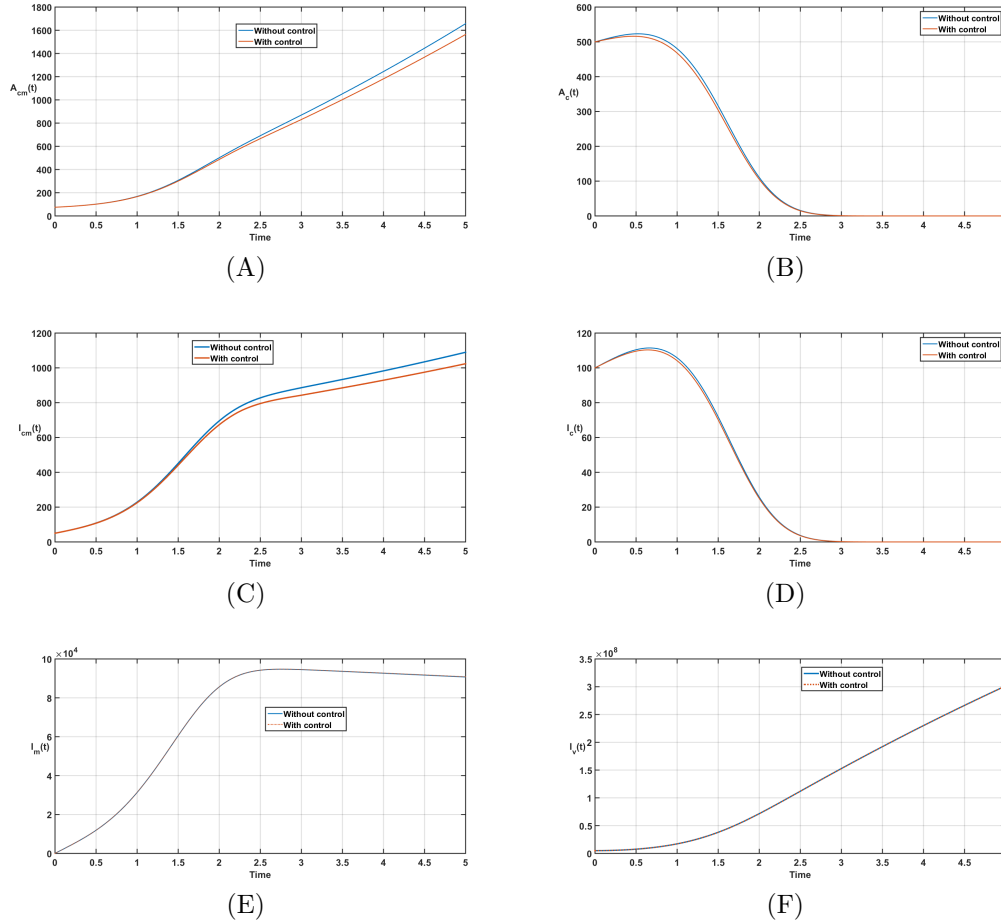
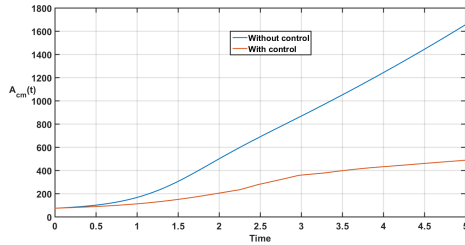
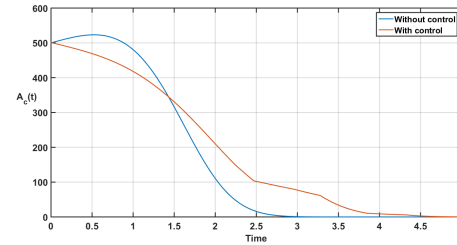


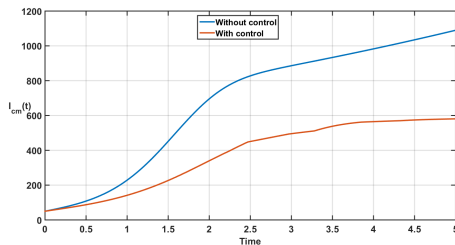
Figure 22: The time-series of infected compartments when the strategy w_{14} is used only.



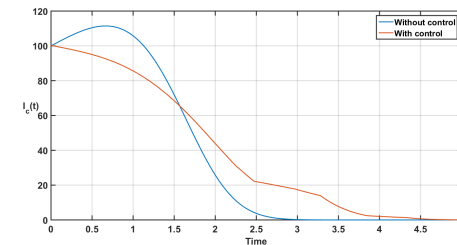
(A)



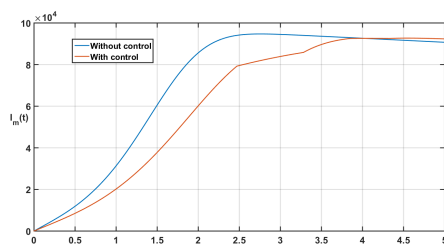
(B)



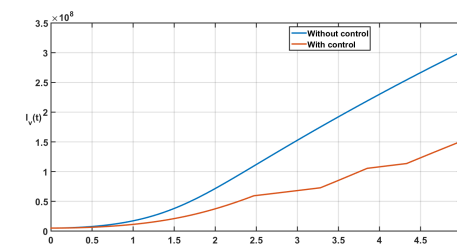
(C)



(D)

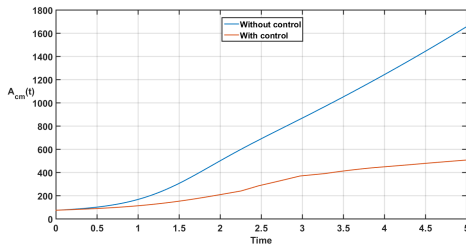


(E)

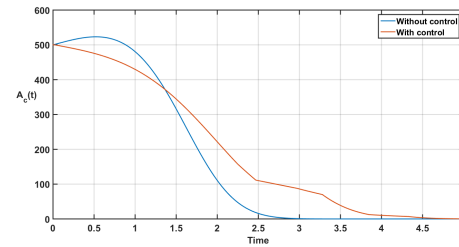


(F)

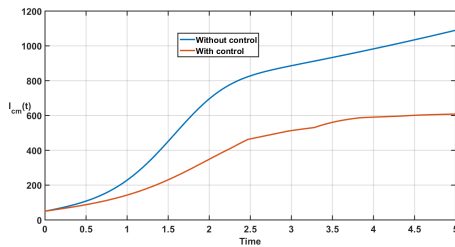
Figure 23: The time-series of infected compartments when the strategy w_{15} is used only.



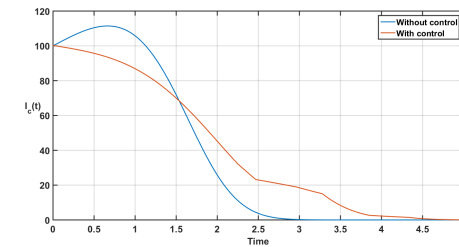
(A)



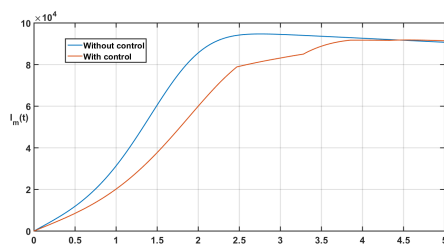
(B)



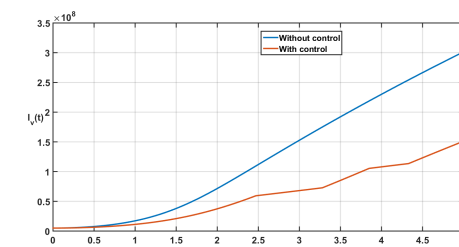
(C)



(D)



(E)



(F)

Figure 24: The time-series of infected compartments when the strategy w_{16} is used only.

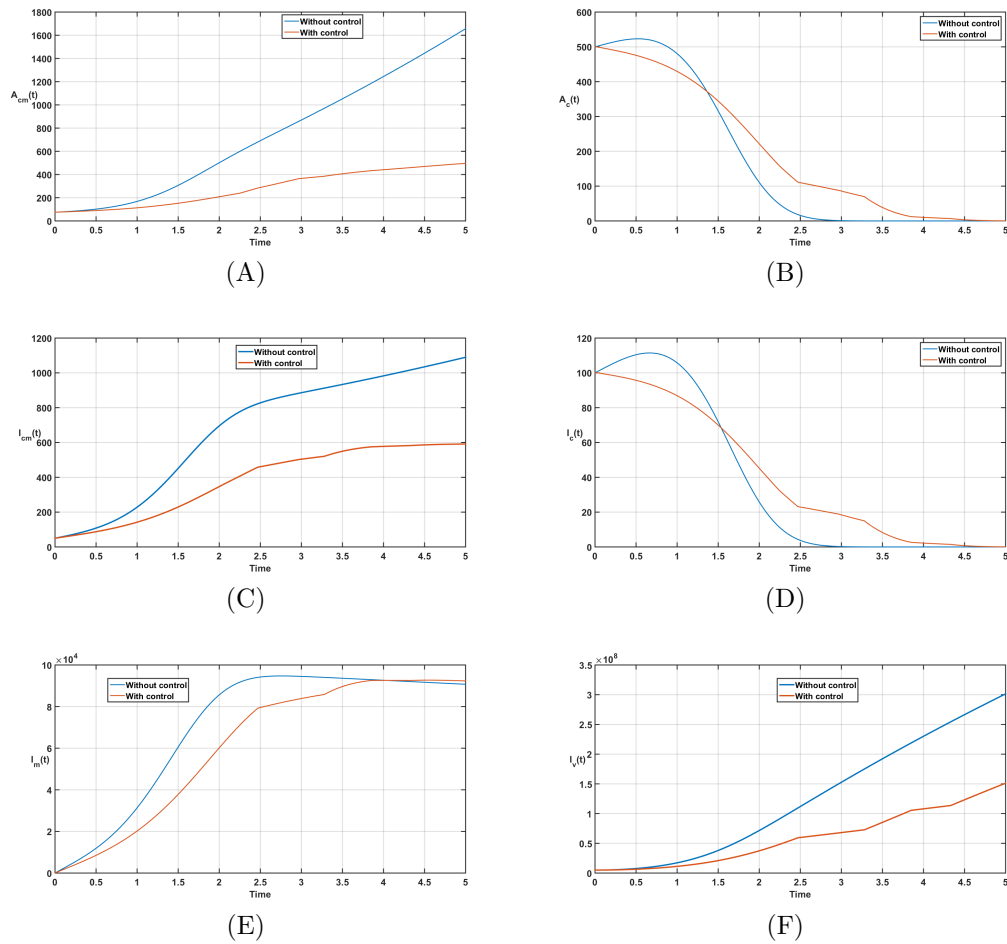


Figure 25: The time-series of infected compartments when the strategy w_{17} is used only.

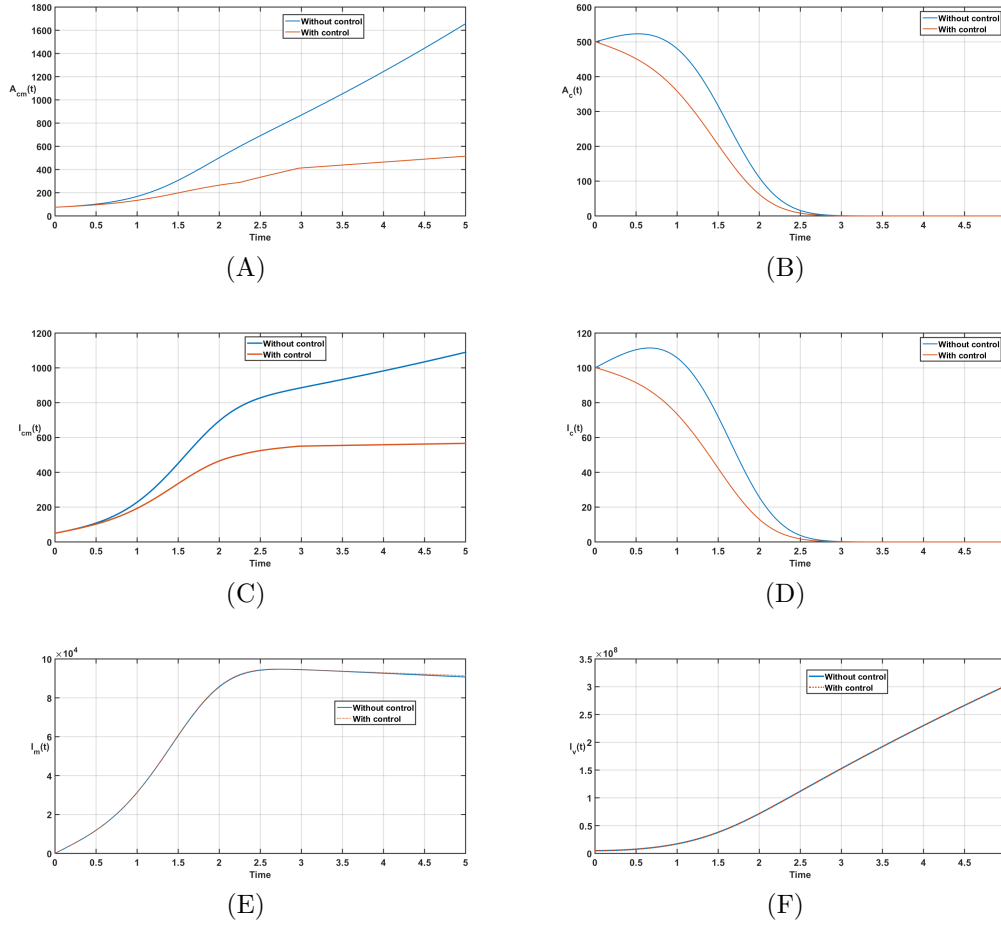


Figure 26: The time-series of infected compartments when the strategy w_{18} is used only.

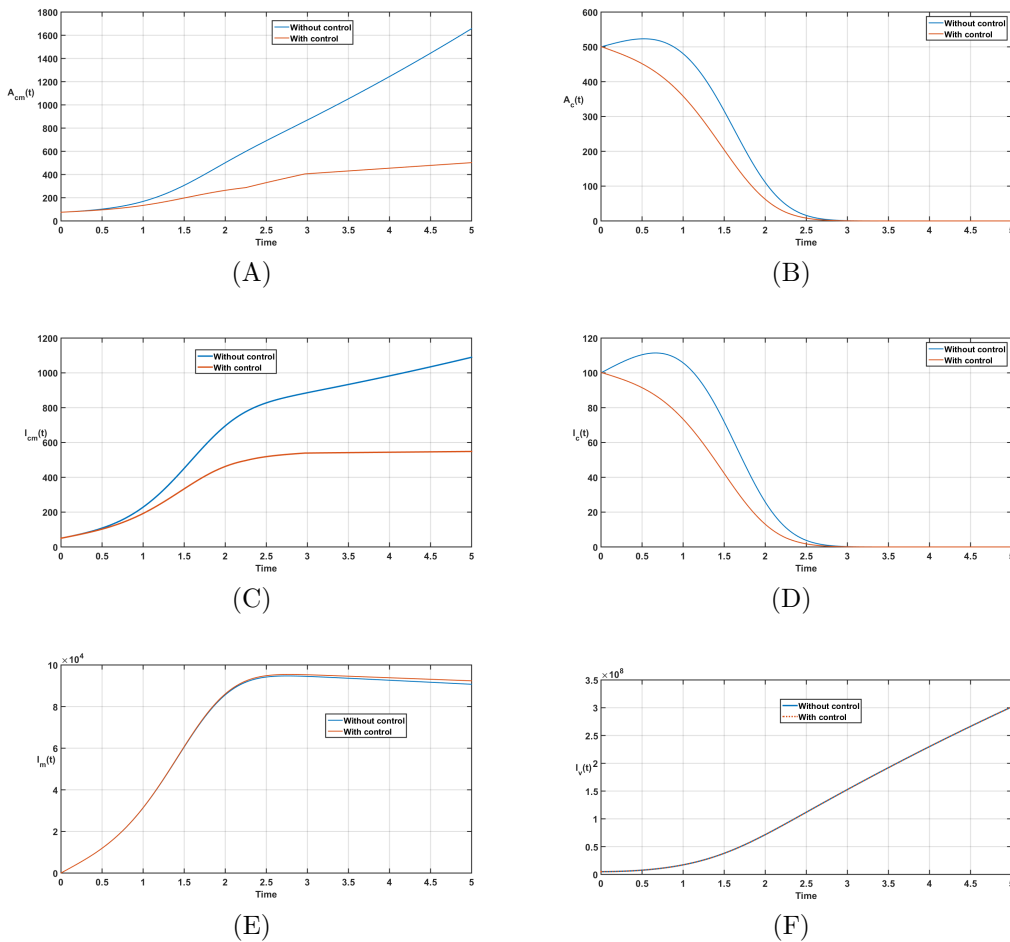
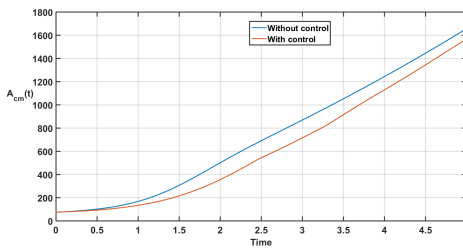
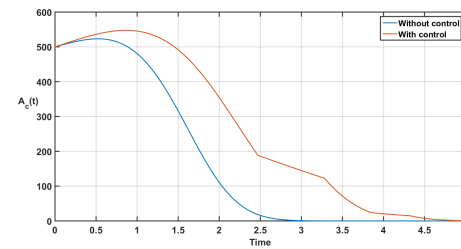


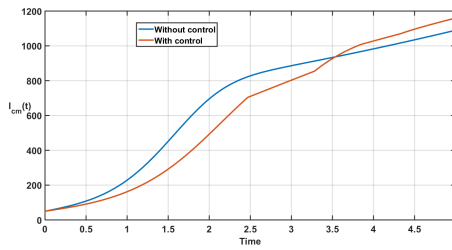
Figure 27: The time-series of infected compartments when the strategy w_{19} is used only.



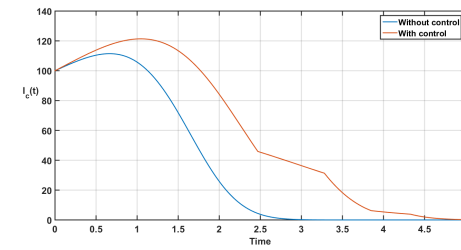
(A)



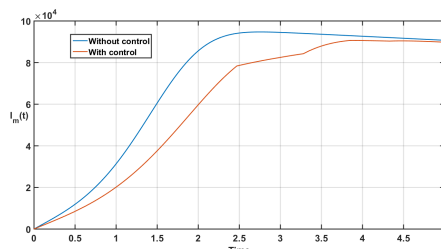
(B)



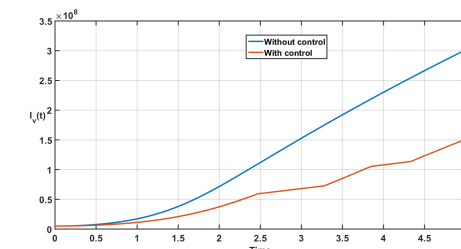
(C)



(D)

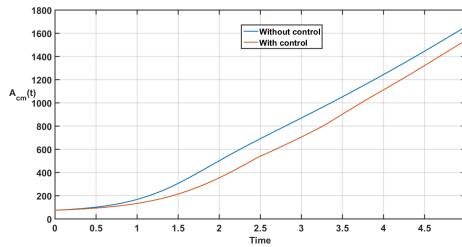


(E)

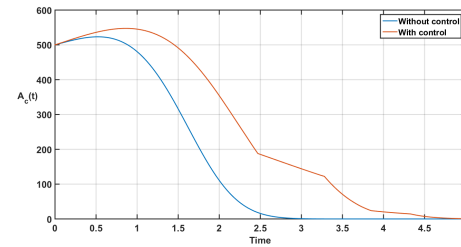


(F)

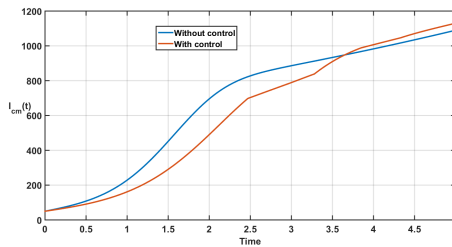
Figure 28: The time-series of infected compartments when the strategy w_{20} is used only.



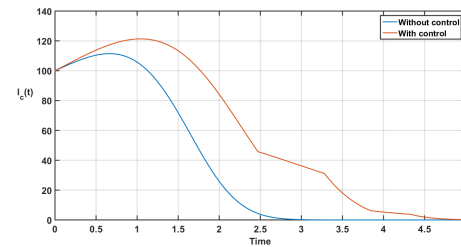
(A)



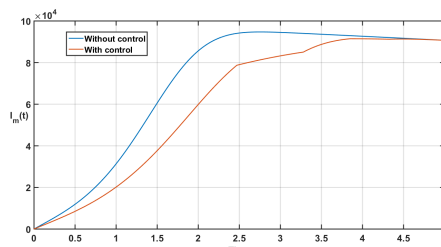
(B)



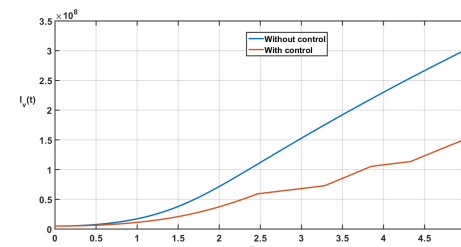
(C)



(D)



(E)



(F)

Figure 29: The time-series of infected compartments when the strategy w_{21} is used only.

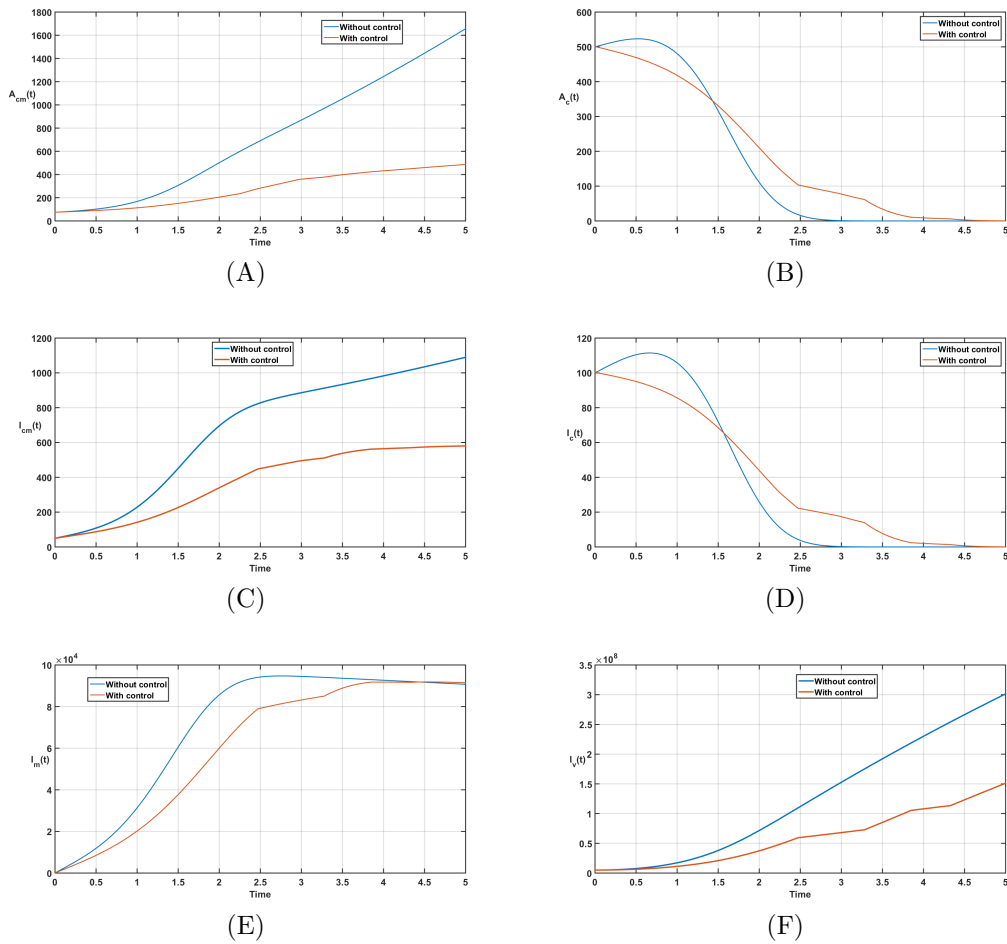


Figure 30: The time-series of infected compartments when the strategy w_{22} is used only.

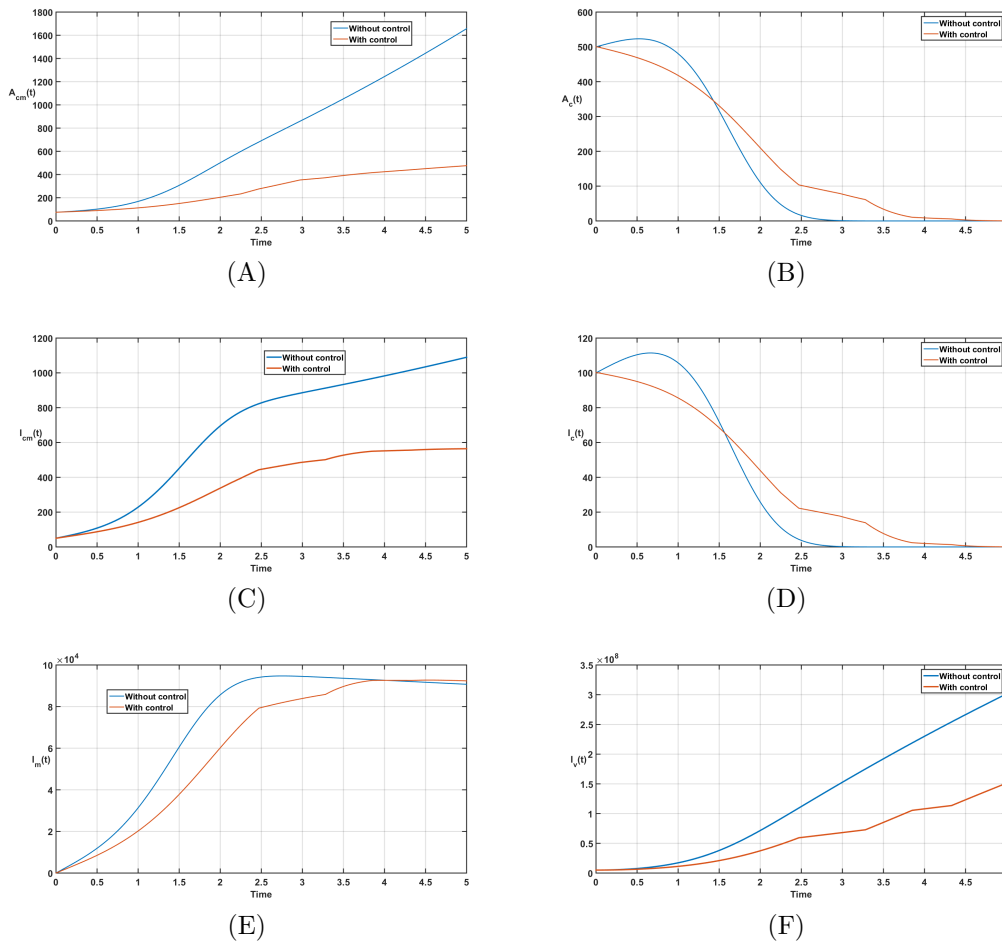


Figure 31: The time-series of infected compartments when the strategy w_{23} is used only.

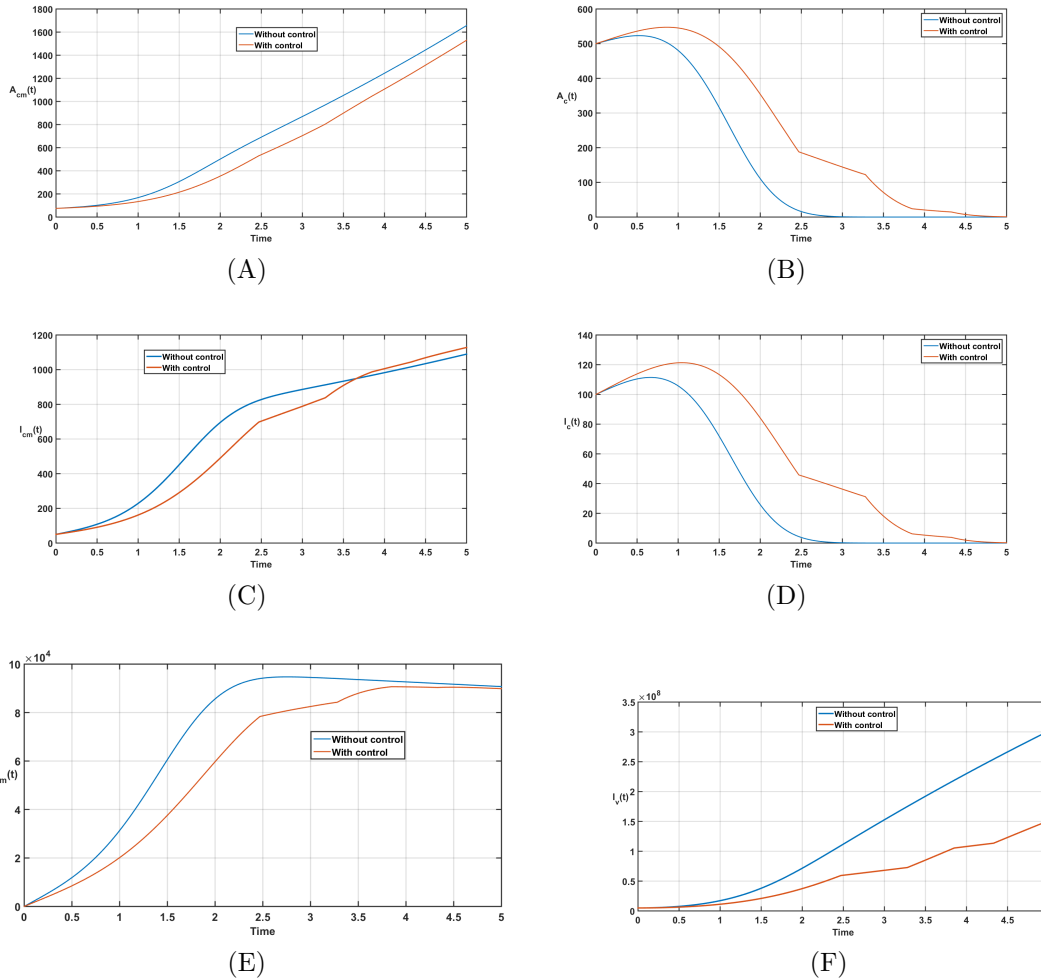


Figure 32: The time-series of infected compartments when the strategy w_{24} is used only.

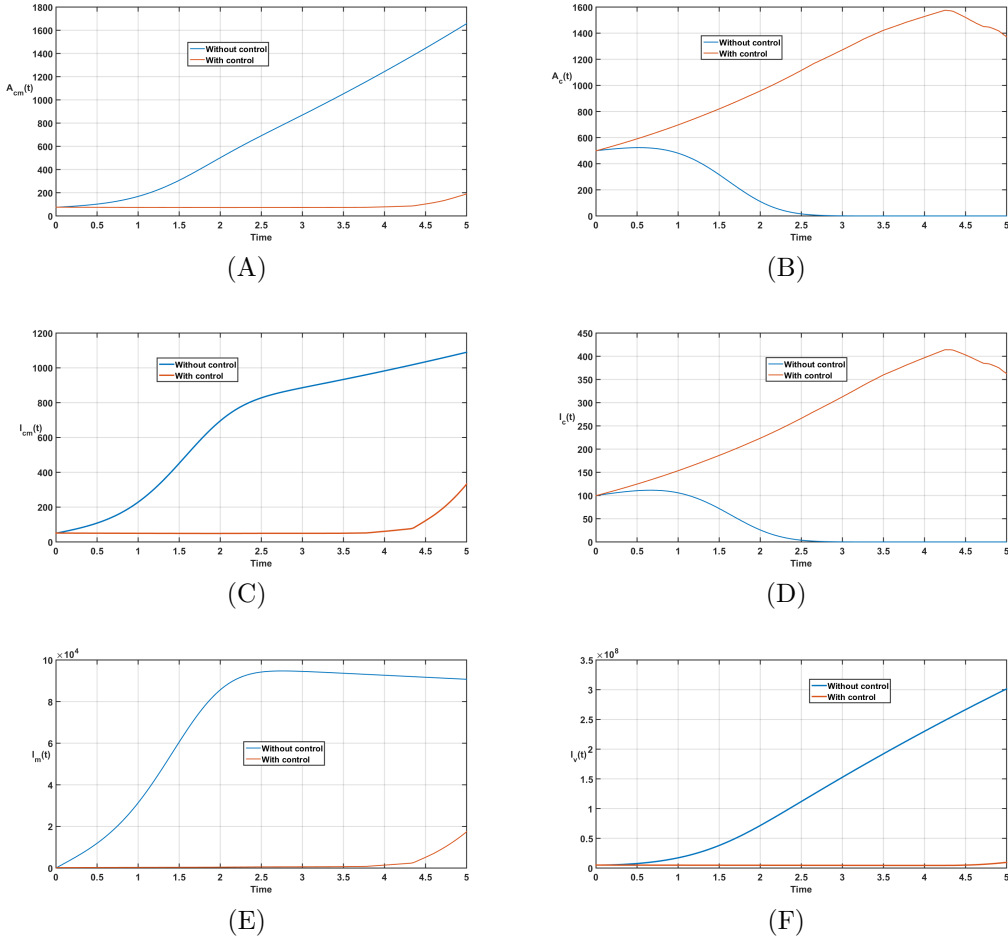


Figure 33: The time-series of infected compartments when we combine all the controls (strategy w_{25}), i.e. $u_i \neq 0$, $i = 1, 2, \dots, 5$.

1
2
3
4
5 **5. Concluding remarks**

6 In this study, we conducted a thorough analysis and development of a model to examine
7 the transmission of co-infection between COVID-19 and malaria. The model encompassed
8 preventive measures, treatments for infected individuals, and an optimal control analysis.
9 Through this analysis, we gained valuable insights into the qualitative dynamics of the co-
10 infection, leading to the following results:

- 11 (i) The COVID-19 model exhibited a locally stable disease-free equilibrium when the
12 reproduction number (\mathcal{R}_{0c}) was less than one ($\mathcal{R}_{0c} < 1$), but it became unstable
13 otherwise.
- 14 (ii) The malaria model demonstrated a stable (in the sense of local steadiness) disease-free
15 equilibrium when the reproduction number (\mathcal{R}_{0m}) was $<$ one, while it became unstable
16 when R_{0m} was greater than one ($\mathcal{R}_{0m} > 1$).
- 17 (iii) The COVID-19 model showed asymptotically stable disease-free equilibrium globally
18 whenever \mathcal{R}_i was less than or equal to one, and unstable otherwise.
- 19 (iv) The malaria model demonstrated asymptotically stable disease-free equilibrium glob-
20 ally whenever \mathcal{R}_{om} was less than or equal to one, and unstable otherwise.
- 21 (v) Our analysis revealed that COVID-19 infection is related with an increased risk of
22 malaria, and vice versa.
- 23 (vi) Solely focusing on COVID-19 intervention strategies, such as optimal preventions and
24 treatments, without simultaneously addressing malaria control, would not effectively
25 control either COVID-19 or malaria in the long run. Similar results were obtained
26 when focusing solely on malaria intervention strategies.
- 27 (vii) Co-infected individuals with both COVID-19 and malaria experience a higher disease
28 burden and greater severity compared to individuals infected with COVID-19 only or
29 malaria only.
- 30 (viii) Implementing multiple control measures simultaneously (using all control measures
31 u_1, u_2, u_3, u_4, u_5) significantly contributes to the effective control of COVID-19, malaria,
32 and infections with both COVID-19 and malaria.

33
34 **References**

- 35 [1] H.A.Rothan, S.N. Byrareddy, The epidemiology and pathogenesis of coronavirus dis-
36 ease (COVID-19) outbreak, J. Autoimmunity. 109 (2020) 102433.
- 37 [2] S.Zhao, Q. Lin, J. Ran, S.S Musa, G.Yang, W. Wang, Y. Lou, D. Gao, L. Yang, D.
38 He, M.H. Wang, Preliminary estimation of the basic reproduction number of novel
39 coronavirus (2019-nCoV) in China, from 2019 to 2020: A data-driven analysis in the
40 early phase of the outbreak, Int. J. Infect. Dis. 92(2021) 214-217.
- 41 [3] WHO (2023) World Health Organization. <https://covid19.who.int/>
- 42 [4] WHO (2019) World Health Organization. World malaria report 2019. Geneva: WHO;
43 2019. <https://www.who.int/publications/item/world-malaria-report-2019>.

- [5] J.M. Tchuenche, C. Chiyaka, D.Chan, A. Matthews, G. Mayer, A mathematical model for antimalarial drug resistance, *Math. Med. Biol.* (2010) 1–21.
- [6] R. Ansumana, O. Sankoh, A. Zumla, Effects of disruption from COVID-19 on anti-malarial strategies, *Nat. Med.* 26(2020) 1334–1336.
- [7] J.R.Gutman, N.W. Lucchi, P.T. Cantey, L.C. Steinhardt, A.M. Samuels, M.L. Kamb, B.K. Kapella, P.D. McElroy, V. Udhayakumar, K.A. Lindblade, Malaria and parasitic neglected tropical diseases: potential syndemics with COVID-19? *Am J Trop Med Hyg* 103(2020) 572–577.
- [8] G.F. Killeen, T.A. Smith, H.M. Ferguson, H. Mshinda, S. Abdulla, C. Lengeler, S.P. Kachur., Preventing childhood malaria in Africa by protecting adults from mosquitoes with insecticide-treated nets, *PLoS Med.* 2007, 4,e229.
- [9] N Chitnis, J.M. Hyman, Crushing, Determining important parameters in the spread of malaria through the sensitivity analysis of a mathematical model, *Bullet. mathcal. Biol.* 70(2008), 1272-1296.
- [10] Z. Hu, C. Song, C. Xu, G. Jin, Y. Chen, X. Xu, H. Ma, W. Chen, Y. Lin, Y. Zheng, J. Wang, Clinical characteristics of 24 asymptomatic infections with COVID-19 screened among close contacts in nanjing, China. *Sci. China Life Sci.* 63(2020) 706–711
- [11] S. Barbosa, I.M. Hastings, The importance of modelling the spread of insecticide resistance in a heterogeneous environment: the example of adding synergists to bed nets, *Malari. J.* 11(2012) .
- [12] P.L. Birget, J.C. Koella. A genetic model of the effects of insecticide-treated bed nets on the evolution of insecticide-resistance. *Evolutionary Med.. Publ. Healt.* (2015) 205–215.
- [13] M.O. Adewole, A.A. Onifade, F.A. Abdullah, F. Kasali, A.I.M. Ismail AIM. Modeling the Dynamics of COVID-19 in Nigeria. *Int J. Appl. Comput. Math.* 67(2021) <https://doi.org/10.1007/s40819-021-01014-5>.
- [14] L. Xiang, M. Tang, Z. Yin, M. Zheng, S. Lu, The COVID-19 pandemic and economic growth: theory and simulation, *Front. Publ. Heal.* 9(2021), 741525. 10.3389/fpubh.2021.741525 [PubMed: 34604164]
- [15] J. Bai, X. Wang, J. Wang. An epidemic-economic model for COVID-19. *Math. Biosci. Eng.* 19(2022) 9658–9696. doi:10.3934/mbe.2022449.
- [16] S.Y. Tchoumi, M.L. Diagne, H. Rwezaura, J.M. Tchuenche. Malaria and COVID-19 co-dynamics: A mathematical model and optimal control. *Appl. Mathcal. Model.* 99(2021) 294–327.
- [17] M.M. Ojo, E.F. Doungmo. The impact of COVID-19 on a malaria dominated region. A mathematical analysis and simulations. *Alex Eng J.* 65 (2023) 23-39.
- [18] N. Chitnis, J.M. Cushing, J.M. Hyman. Bifurcation analysis of a Mathematical model for malaria transmission. *SIAM. J. Appl. Math.* 67(2006) 24-45.

- [19] WHO, Insecticide-treated Mosquito Nets: A WHO Position Statement. Global Malaria Programme (2007)
- [20] F.O. Okumu, S.S. Kiware, S.J. Moore, G.F. Killeen, Mathematical evaluation of community level impact of combining bed net sand indoor residual spraying upon malaria transmission in areas where the main vectors are *Anopheles arabiensis* mosquitoes, *Parasit. Vects.* 17(2013).
- [21] World Bank Data, Life expectancy at birth, total (years) - Sub-Saharan Africa iseases. New Yor. Springer-Verlag 859(2020).
- [22] S. Djaoue, G.G. Kolaye, H. Abboubakar, A.A.A. Ari, I. Damakoa, Mathematical modeling, analysis and numerical simulation of the COVID-19 transmission with mitigation of control strategies used in Cameroon. *Cha. Solit. Fract.* 138(2020) 110281
- [23] M. Day, Covid-19. four fifths of cases are asymptomatic, China figures indicate, *Br. Med. J.* 2369(2020)
- [24] B. Buonomo. Analysis of a malaria model with mosquito host choice and bed-net control, *Int. J. Biomath.* 8(2015).
- [25] T.A. Adnan, H. Abboubakar, K. Aziz, A. Thabet. Mathematical modeling of the COVID-19 epidemic with fear impact, *AIMS. Math.* 8(2023) 6447-6465
- [26] J.K. Osoro, M.G. Machani, E. Ochomo, C. Wanjala, E. Omukunda, A.K. Githeko, G. Yan, Y.A. Afrane, Insecticide resistant *anopheles gambiae* have enhanced longevity but reduced reproductive fitness and a longer first gonotrophic cycle, *Scientific reports*, 12(2022) 1–7.
- [27] L.G. Molineaux, J. Shidrawi, J. Clarke, T.A. Boulzaguet, Assessment of insecticidal impact on the malaria mosquito's vectorial capacity, from data on the man-biting rate and age-composition, *Bullet. WHO.* (1978) 57265.
- [28] R. N'Guessan, V. Corbel, M. Akogbeto, M. Rowland, Reduced efficacy of insecticide-treated nets and indoor residual spraying for malaria control in pyrethroid resistance area, Benin, *Emerging infectious diseases.* 2007, 13:199.
- [29] World Health Organization (WHO), (2012). Global Malaria Programme. Worl. Malari. Rep.
- [30] F.U. Dyah, P.J. Nainggolan. Parameter Estimation and Sensitivity Analysis of Malaria Model. *Journal of Physics: Conf. Seri.* 1490(2020) 012039. doi:10.1088/1742-6596/1490/1/012039.
- [31] J.P. Lassalle . The stability of dynamical systems, Philadephia. SIAM. 34(1976) 56-68.
- [32] W.H. Fleming, R.W. Rishel. Deterministic and Stochastic Optimal Control, Spring. Verl. Nw. Yor. 1975.
- [33] E. Sherrard-Smith, A.B. Hogan, A. Hamlet, O.J. Watson, C. Whittaker, P. Winskill et al. The potential public health conse-361 quences of COVID-19 on malaria in Africa. *Nat. Med.* (2020) doi.org/10.1038/s41591-020-1025-y.

- 1
2
3 [34] S. Lenhart, J.T. Workman. Optimal Control Applied to Biological Models, Chapma.
4 Hal. (2007).
5
6 [35] M.M. Plucinski, T. Guilavogui, S. Sidikiba et al. Effect of the Ebolavirus disease epi-
7 demic on malaria case management in Guinea, 2014: a cross-sectional survey of health
8 facilities. Lancet. Infect. Dis. 407(2015) 1017-23
9
10
11
12
13
14
15
16
17
18
19
20
21
22
23
24
25
26
27
28
29
30
31
32
33
34
35
36
37
38
39
40
41
42
43
44
45
46
47
48
49
50
51
52
53
54
55
56
57
58
59
60
61
62
63
64
65